Acta Neuropathologica Communications

RESEARCH

Open Access

Ablation of progranulin augments microglial activation and accelerates prion progression

Bei Li[1†], Yiyue Shi[1†], Wenyu Hou[1†], Haoyuan Guan[1], Jun Li[1], Tuo Yi[1], Wei Li[1], Donglin Cai[1], Petra Schwarz[2], Adriano Aguzzi[2*] and Caihong Zhu[1*]

Abstract

Mutations or polymorphisms in *GRN*, encoding the CNS glycoprotein progranulin (PGRN), have been linked to several neurodegenerative diseases. In this study, we explored the role of PGRN in prion diseases. We observed that prion infection upregulated microglial PGRN expression. Following intracerebral inoculation with RML6 prions, $Grn^{-/-}$ mice exhibited accelerated disease progression compared to $Grn^{+/-}$ and $Grn^{+/+}$ littermates. Histological analysis revealed augmented microglial activation in $Grn^{-/-}$ mice. Temporal analysis revealed enhanced early microglial activation and prion clearance at 120 dpi, followed by excessive complement activation but inadequate clearance by 150 dpi. Additionally, $Grn^{-/-}$ brains exhibited exacerbated astrogliosis and vacuolation. RNA-seq analysis indicated that complete PGRN deficiency in prion-infected mice shifted microglia from homeostatic to pro-inflammatory states. Notably, microglia-specific depletion of PGRN did not affect prion pathogenesis, suggesting that PGRN deficiency affects microglial activation and prion progression in a non-cell autonomous manner. These findings suggest that microglia respond to prion infection in a stepwise manner, and PGRN plays a critical role in modulating prion-induced microglial activation. Our results highlight the neuroprotective role of PGRN in prion disease and suggest that supplementation or boosting expression of PGRN could represent a promising therapeutic strategy.

Keywords Progranulin, Prion disease, Microglia, Neuroinflammation, Neurodegeneration

Introduction

Progranulin (PGRN), encoded by the *GRN* gene, is a glycoprotein involved in diverse biological processes, including development, wound healing, and tumorigenesis [1]. In the central nervous system (CNS), PGRN is predominantly expressed by microglia and neurons, where it functions as a neurotrophic factor to promote neuronal development, survival and neurite growth [2, 3]. In 2006, several independent studies identified that loss-of-function mutations in *GRN* gene, leading to haploinsufficiency, cause frontotemporal lobar degeneration (FTLD) with tau-negative, ubiquitin-positive inclusions [4–6]. These inclusions were later found to contain transactivation response DNA binding protein-43 (TDP-43) [7, 8]. PGRN is not only secreted but also localizes

†Bei Li, Yiyue Shi and Wenyu Hou contributed equally to this work.

*Correspondence:
Adriano Aguzzi
Adriano.Aguzzi@uzh.ch
Caihong Zhu
Caihong_Zhu@fudan.edu.cn
[1]School of Basic Medical Sciences, State Key Laboratory of Brain Function and Disorders, Fudan University, Dong'An Rd 130, Shanghai 200032, China
[2]Institute of Neuropathology, University of Zurich, Schmelzbergstrasse 12, Zurich CH-8091, Switzerland

to lysosomes, where it plays a critical role in lysosomal functions [9, 10]. Homozygous *GRN* mutations have been linked to lysosomal storage disorders, such as neuronal ceroid lipofuscinosis (NCLs) [11–16]. Furthermore, genome-wide association studies (GWAS) have identified *GRN* variants as risk factors for a broad spectrum of neurodegenerative diseases, including Alzheimer's disease (AD) [17–26], Parkinson's disease (PD) [27], amyotrophic lateral sclerosis (ALS) [28], corticobasal syndrome (CBS) [29, 30], limbic-predominant aging-related TDP-43 encephalopathy (LATE) [31], and Lewy body dementia [32]. However, the mechanisms by which *GRN* mutations or variants contribute to neurodegeneration remain poorly understood.

Grn knockout mice have been widely used to dissect PGRN's functions and the mechanisms underlying PGRN deficiency-associated neurodegeneration [33–37]. While $Grn^{+/-}$ mice are neuropathologically indistinguishable from wild type mice, $Grn^{-/-}$ mice consistently develop microglial activation, astrogliosis, neuronal loss and accelerated lipofuscinosis with aging [37, 38]. These findings suggest that PGRN acts as a brake, suppressing aberrant microglial activation and controlling neuroinflammation during aging or under pathological conditions [34, 37]. Notably, ubiquitinated and phosphorylated TDP-43 aggregates are also observed in aged $Grn^{-/-}$ mice [36, 37]. Mechanistically, PGRN is implicated in the autophagy-lysosomal pathway, and its deficiency may impair autophagy and lysosomal homeostasis, leading to TDP-43 accumulation [39, 40]. Single-nucleus RNA-sequencing (snRNA-seq) of $Grn^{-/-}$ mouse brains revealed that microglia are the first cells to exhibit transcriptomic changes, transitioning from a homeostatic to a disease-associated phenotype [41, 42]. Additionally, PGRN deficiency in microglia have been linked to altered lipid metabolism [43–46]. Recent studies using snRNA-seq have also identified neurovascular dysfunction in FTD-GRN patients [47]. In animal models of neurodegenerative disease, PGRN deficiency exacerbates MPTP-induced dopaminergic neuronal loss and accelerates tau deposition and phosphorylation in human tau-expressing mice [34, 48, 49]. Interestingly, in mouse models of AD, PGRN deficiency has been reported to either increase Aβ deposition [50, 51] or decrease diffuse Aβ plaques [49, 52]. The reasons for these discrepancies remain unclear but may be attributed to differences in mouse models and/or the ages of animals studied.

Prion diseases are a group of fatal neurodegenerative disorders affecting both animals and humans [53]. Prion diseases remain incurable, with pathological hallmarks including spongiform changes, deposition of scrapie prion protein (PrP^{Sc}), and prominent microglial activation [54]. Microglia play an overall neuroprotective role in prion diseases by clearing prions in the brain [55]. Microglia-derived triggering receptor expressed on myeloid cells 2 (TREM2) has been implicated in prion-induced microglial activation [56], but the molecular mechanisms underlying microglial activation and prion clearance remain to be dissected. Autophagic and lysosomal abnormalities have been observed in both patients and animal models of prion diseases [57, 58], yet the contribution of impaired autophagy and lysosomal dysfunction to prion-induced neurodegeneration is not fully elucidated. Given PGRN's involvement in various neurodegenerative disorders, particularly through its regulation of autophagy and lysosomal functions in microglia, we sought to determine whether PGRN plays a role in prion pathogenesis.

In this study, we first assessed PGRN expression in prion-infected mouse brains and found that it was significantly upregulated in microglia following prion infection. Prion inoculation experiments revealed that complete PGRN deficiency ($Grn^{-/-}$) accelerated disease progression compared to heterozygous ($Grn^{+/-}$) and wild-type ($Grn^{+/+}$) littermates. Histological analysis demonstrated that $Grn^{-/-}$ microglia exhibited aberrant activation, adopting an amoeboid morphology and displaying altered cytokine profiles. At 120 days post-inoculation (dpi) of prion, $Grn^{-/-}$ microglia were more activated and efficient at clearing prions, resulting in reduced prion deposition. However, by 150 dpi, overactivated $Grn^{-/-}$ microglia triggered excessive complement activation and insufficient prion clearance, leading to PrP^{Sc} levels comparable to those in $Grn^{+/-}$ and wild-type littermates. RNA-seq analysis revealed that complete PGRN deficiency in prion-infected mice shifted microglia from a homeostatic to a disease-associated phenotype. Interestingly, microglia-specific depletion of *Grn* did not affect prion pathogenesis. These findings suggest that microglia respond to prion infection in a stepwise manner, and complete PGRN deficiency sensitizes mice to prion-induced neurodegeneration. PGRN restricts prion-induced microglial activation and protects against prion diseases, partly by suppressing excessive activation of complement cascade.

Materials and methods

Ethical statement

All animal experiments were carried out in strict accordance with the Rules and Regulations for the Protection of Animal Rights (Tierschutzgesetz and Tierschutzverordnung) of the Swiss Bundesamt für Lebensmittelsicherheit und Veterinärwesen and were preemptively approved by the Animal Welfare Committee of the Canton of Zürich (permit ZH040/2015).

Animals

$Grn^{-/-}$ mice [33] carrying a targeted deletion of exons 2–13 were first backcrossed to C57BL/6J to obtain

Grn$^{+/-}$ offspring. *Grn*$^{+/-}$ mice were then intercrossed to obtain *Grn*$^{-/-}$, Grn$^{+/-}$ and *Grn*$^{+/+}$ (WT) littermates, which were used for the experiments described here. CX3CR1-CreERT2 mice expressing tamoxifen inducible Cre under endogenous CX3CR1 promoter were purchased from Jackson's lab (JAX Stock #021160) [59]. *Grn*$^{fl/fl}$ mice with the whole coding sequence floxed [34] were crossed to CX3CR1-CreERT2 mice to generate CX3CR1-CreERT2; *Grn*$^{fl/fl}$ mice. *Prnp*$^{-/-}$ mice [60] kept on a C57BL/6J background were used as prion-resistant controls.

Mice were maintained in high hygienic grade facility and housed in groups of 3–5, under a 12 h light/12 h dark cycle (from 7 am to 7 pm) at 21 ± 1 °C, with sterilized food (Kliba No. 3242, Provimi Kliba, Kaiseraugst, Switzerland) and water *ad libitum*.

Generation of Grn$^{-/-}$ BV2 cells

Cells were cultured in Dulbecco's Modified Eagle Medium (DMEM; MeilunBio, MA0212) supplemented with 10% fetal bovine serum (FBS; MeilunBio, PWL217), 1% L-glutamine (MeilunBio, PWL031), 1% penicillin-streptomycin (MeilunBio, MA0110) at 37 °C with 5% CO_2.

To generate *Grn*$^{-/-}$ BV2 cells, single guide RNAs (sgRNAs) targeting the mouse *Grn* gene were designed using CRISPOR (http://crispor.tefor.net/). The sgRNA oligonucleotides (forward: 5′-CAC CGC TGG CTG GCC TTC GCG GCA GT-3′, reverse: 5′-TAA AAC TGC CGC GAA GGC CAG CCA GC-3′) were synthesized and cloned into the LentiV2 CRISPR/Cas9 vector. Lentiviral particles were produced in HEK293T cells by co-transfecting LentiV2-*Grn* plasmid (6 μg) with the packaging plasmids PMD2.G (4 μg) and pSPAX2 (3 μg), and applied to BV2 cells that had been pre-seeded in 6-well plates. 48 h post-transduction, the culture medium was replaced with complete medium containing puromycin (2 μg/mL) for selection for 5 days. Successful generation of *Grn*$^{-/-}$ BV2 cells were verified by DNA sequencing of the *Grn* target site and Western blot.

Intracerebral prion inoculation

Grn$^{-/-}$ (8 female, 10 male), *Grn*$^{+/-}$ (14 female, 11 male) and *Grn*$^{+/+}$ (WT) (11 female, 4 male) mice at 1.5-2 months old were intracerebrally (i.c) inoculated with 30 μl of 0.1% (w/v) brain homogenate diluted in PBS with 5% BSA and containing 3 × 10^5 LD50 units of the RML6. For CX3CR1-CreERT2; *Grn*$^{fl/fl}$ mice (13 female, 12 male) and *Grn*$^{fl/fl}$ controls (12 female, 13 male), mice at 1 month old were first fed with Tamoxifen diet (ENVIGO, TD.55125IC.I Tam400/CreER, Tamoxifen Citrate 400 ppm) for 4 weeks, followed by normal food (Kliba No. 3242) to rest for 2 weeks. CX3CR1-CreERT2; *Grn*$^{fl/fl}$ mice (12 female, 12 male) and *Grn*$^{fl/fl}$ controls (13 female, 11 male) without Tamoxifen diet feeding were also used for control. Then mice were i.c inoculated with 30 μl RML6. Scrapie was diagnosed according to clinical criteria (ataxia, kyphosis, priapism, and hind leg paresis) as previously described [61]. Briefly, mice were observed every other day after RML6 inoculation for clinical signs including gait, grooming, activity, rough hair coat, limb paresis and ataxia. Once the mice showed the first sign of scrapie (grade 1: wadding gait, mild signs of reduced grooming, rough hair coat, limb weakness, front leg paresis, etc.), they were monitored every day and wet food was supplied in the cage. When the mice reached score grade 2 (ataxia, reduced grooming and activity, paralysis and rolling, etc.) that hamper the mice reaching water bottle, they were defined as terminally sick. Mice were sacrificed at various time points for analysis at pre-clinical and clinical stages, and on the day of onset of terminal clinical signs of scrapie. Non-infectious brain homogenates (NBH) prepared from uninfected mice and diluted with the same concentration (0.1%) as RML6 were used as negative controls.

Quantitative real-time PCR (qRT-PCR)

Total RNA from brain was extracted using TRIzol (Invitrogen Life Technologies) according to the manufacturer's instruction. The quality of RNA was analyzed by Bioanalyzer 2100 (Agilent Technologies), RNAs with RNA integrity number > 7 were used for cDNA synthesis. cDNA was synthesized from ~ 1 μg total RNA using QuantiTect Reverse Transcription kit (QIAGEN) according to the manufacturer's instruction. Quantitative real-time PCR (qRT-PCR) was performed using the SYBR Green PCR Master Mix (Roche) on a ViiA7 Real-Time PCR system (Applied Biosystems).

The following primer pairs were used: *Gapdh* sense 5′-CCA CCC CAG CAA GGA GAC T-3′; antisense, 5′-GAA ATT GTG AGG GAG ATG CT-3′. *Grn* sense 5′- GTG TTG TGA GGA TCA CAT TC -3′; antisense, 5′- CTA TGA CCT TCT TCA TCC AG -3′. *Tnfα* sense, 5′-CAT CTT CTC AAA ATT CGA GTG ACA A-3′; antisense, 5′-TGG GAG TAG ACA AGG TAC AAC CC-3′. *Il-1β* sense, 5′-CAA CCA ACA AGT GAT ATT CTC CAT G-3′; antisense, 5′-GAT CCA CAC TCT CCA GCT GCA-3′. *Il-6* sense, 5′-TCC AAT GCT CTC CTA ACA GAT AAG-3′; antisense, 5′-CAA GAT GAA TTG GAT GGT CTT G -3′. *C1qa* sense, 5′-AAA GGC AAT CCA GGC AAT ATC A-3′; antisense, 5′-TGG TTC TGG TAT GGA CTC TCC-3′. *C3* sense, 5′-CCA GCT CCC CAT TAG CTC TG-3′; antisense, 5′-GCA CTT GCC TCT TTA GGA AGT C-3′. *Cd22* sense, 5′-CCA CTC CTC AGG CCA GAA ACT-3′; antisense, 5′-TGC CGA TGG TCT CTG GAC TG-3′.

Western blot analysis

Forebrains of one hemisphere from prion-infected mice were homogenized in sterile 0.32 M sucrose in PBS. Total protein concentration was determined using the bicinchoninic acid assay (Pierce). ~20 µg proteins were loaded and separated on a 12% Bis-Tris polyacrylamide gel (NuPAGE, Invitrogen) and then blotted onto a nitrocellulose membrane. Membranes were blocked with 5% Topblock (LuBioScience) (w/v) in PBS supplemented with 0.05% Tween 20 (v/v) and incubated with primary antibodies in 1% Topblock overnight at 4 °C. After washing, the membranes were then incubated with horseradish peroxidase (HRP)-conjugated secondary antibodies for 2 h at room temperature. Blots were developed using Luminata Crescendo Western HRP substrate (Millipore) and visualized using the FUJIFILM LAS-3000 system. Primary antibodies used in this study included anti-PGRN antibody (1:400, R&D system, AF2557), POM1 (200 ng ml^{-1}), anti-Iba1 (1:1,000, Wako laboratory chemicals, 019-19741), anti-GFAP (1:2,000, Cell signaling technology, 12389 S), anti-C1qa (1:1,000, Abcam, ab71089), anti-C3 (1:500, Abcam, ab11862), anti-LC3B (1:1,000, Cell Signaling Technology, 2775 S), anti-P62 (1:1,000, MBL international, PM045). To avoid variation in loading, the same blots were stripped and incubated with an anti-actin (1:10,000, Millipore, MAB1501R) or anti-GAPDH (1:5,000, Millipore, MAB374) antibody. The signals were normalized to actin or GAPDH as a loading control. Secondary antibodies were goat anti-rabbit IgG (1:10,000, Jackson ImmunoResearch, 111-035-045), goat anti–mouse IgG (1:10,000, Jackson ImmunoResearch, 115-035-003), goat anti-rat IgG (1:2,000, Invitrogen, 62-9520) and donkey anti-sheep IgG (1:5,000, Abcam, ab150178).

To detect PrP^{Sc} in prion-infected *Grn*$^{-/-}$, *Grn*$^{+/-}$ and *Grn*$^{+/+}$ (WT) mouse brains, prion-infected forebrains were homogenized in sterile 0.32 M sucrose in PBS. Total protein concentration was determined using the bicinchoninic acid assay (Pierce). Samples were adjusted to 20 µg protein in 20 µl and digested with 25 µg ml^{-1} proteinase K in digestion buffer (PBS containing 0.5% wt/vol sodium deoxycholate and 0.5% vol/vol Nonidet P-40) for 30 min at 37 °C. PK digestion was stopped by adding loading buffer (Invitrogen) and boiling samples at 95 °C for 5 min. Proteins were then separated on a 12% Bis-Tris polyacrylamide gel (NuPAGE, Invitrogen) and blotted onto a nitrocellulose membrane. POM1 (200 ng ml^{-1}) and horseradish peroxidase (HRP)-conjugated goat anti–mouse IgG (1:10,000, Jackson ImmunoResearch, 115-035-003) were used as primary and secondary antibodies, respectively. Blots were developed using Luminata Crescendo Western HRP substrate (Millipore) and visualized using the FUJIFILM LAS-3000 system.

Immunohistochemistry and immunofluorescence staining

For immunohistochemistry of prion-infected brains, formalin-fixed tissues were treated with concentrated formic acid for 60 min to inactivate prion infectivity and embedded in paraffin. Paraffin Sect. (2 µm) of brains were stained with hematoxylin/eosin (H&E). After deparaffinization through graded alcohols, Iba-1 antibody (1:1000; Wako Chemicals GmbH, Germany, 019-19741) was used for highlighting microglial cells, GFAP antibody (1:300; DAKO, Carpinteria, CA, z0334) was used for astrocytes. Stainings were visualized using an IVIEW DAB Detection Kit (Ventana), with a hematoxylin counterstain applied subsequently. For the histological detection of partially proteinase K-resistant prion protein deposition, deparaffinized sections were pretreated with formaldehyde for 30 min and with 98% formic acid for 6 min, and then washed in distilled water for 30 min. Sections were incubated in Ventana buffer and stains were performed on a NEXEX immunohistochemistry robot (Ventana instruments, Switzerland) using an IVIEW DAB Detection Kit (Ventana). After incubation with protease 1 (Ventana) for 16 min, sections were incubated with anti-PrP SAF84 (1:200, SPI bio, A03208) for 32 min. Sections were counterstained with hematoxylin. Sections were imaged using a Zeiss Axiophot light microscope. Quantification of vacuolation (H&E staining), SAF84, GFAP and Iba-1 staining and Sholl analysis were performed on acquired images using Image J software (National Institutes of Health). Briefly, for cell number counting, images were converted into 8-bit grayscale and the thresholds were adjusted to distinguish cells from the background. The particles were then analyzed, and the cell counts and area were measured. The cell counts were also validated by manual counting. For SAF84 signal calculation, images were color deconvoluted and H-DAB was chosen as the stain. The thresholds were adjusted and the mean gray values were measured and analyzed. For Sholl analysis of microglia, images of Iba-1 staining were first converted into 8-bit grayscale and the thresholds were adjusted. After defining a center point in soma, the parameters of Sholl analysis were adjusted. The number of dendritic intersections were counted with different distances from the soma. The operator was blind to the genotype and treatment of the analyzed tissues. 4 ~ 17 sections per group (depending on the samples collected) were used for quantification.

For immunofluorescent staining of PGRN on deparaffinized mouse brain sections, anti-progranulin antibody (10ug ml^{-1}, R&D systems AF2557) and anti-Iba1 (1:1000, Wako laboratory chemicals, 019-19741) were used as primary antibodies and Alexa Fluor® 488 goat anti-rabbit IgG (1:500, Invitrogen, A11008) and Alexa Fluor® 594 donkey anti-sheep IgG (1:500, Abcam, ab150180) were used as secondary antibodies. DAPI was used for

fluorescent nuclear counterstaining. Images were captured using a confocal microscope (Leica, SP8).

ELISA

PGRN levels in tamoxifen-treated *Grn*$^{fl/fl}$ and CX3CR1-CreERT2;*Grn*$^{fl/fl}$ mouse brain samples were determined by an ELISA kit (Abcam, ab213473) according to the manufacturer's protocol. Briefly, forebrain samples of one hemisphere were homogenized in 1X cell extraction buffer PTR to prepare 10% brain homogenates. Total protein concentration was determined using the bicinchoninic acid assay (Pierce). After adjustment of the protein concentration by 1:250 dilution, 50µL samples were loaded to the 96-well plate. The antibody cocktail (50µL) was then added and incubated for 1 h at room temperature. After washing, TMB development solution (100µL) was added to the wells. The reactions were then stopped by stop solution (100µL) and the plate was read at 450 nm. *Grn*$^{-/-}$ mouse brains were used as negative control and background for normalization.

Magnetic activated cell sorting

Mice were anesthetized and perfused with ice-cold PBS. Half brain tissue were collected and immediately put into 10 mL cold D-PBS buffer for microglia isolation. Brains were chopped into small pieces by forceps and transferred to a 70 µm strainer. Tissue were dissociated with a pestle and washed with more D-PBS to collect all cells. Cells were collected by centrifugation at 300×g for 10 min at 4 °C. Pellets were resuspended with 3100 µL of D-PBS + 900 µL Debris Removal Solution, and then slowly and gently overlaid with 4 mL of D-PBS on the top, followed by centrifugation at 4 °C and 3000×g for 10 min with full acceleration and brake. Three phases were formed and the two top phases were aspirated completely to remove myelin and debris. The lower phase was filled with cold D-PBS to a final volume of 15 mL and centrifuged at 4 °C and 1000×g for 10 min with full acceleration and brake. Supernatant were removed completely. Cell pellets were resuspended in 90 µL of cold PB buffer per 10^7 total cells. 10 µL of CD11b (Microglia) MicroBeads (Miltenyi Biotech) were added to the cell suspension and incubated for 15 min in the dark in the refrigerator (2–8 °C). Cells were washed by adding 1 mL of cold PB buffer per 10^7 cells and centrifuged at 300×g for 5 min. Supernatants were removed and cells were resuspended up to 10^7 cells in 500 µL of PB buffer. CD11b$^+$ cells were separated in a magnetic field by MS columns according to the manufacturer's instruction (Miltenyi Biotech). The purity of isolated microglia was analyzed by flow cytometry with CD11b staining. Isolated microglia were immediately lysed in RLT buffer and total RNAs were extracted using RNeasy kit (Qiagen) for further analysis.

RNA sequencing

The quality of RNA extracted from isolated microglia was analyzed by Bioanalyzer 2100 (Agilent Technologies), RNAs with RNA integrity number >8 were further processed. The TruSeq Stranded mRNA Sample Prep Kit (Illumina, Inc, California, USA) was used in the succeeding steps. Briefly, total RNA samples (500 ng) were poly-A selected and then reverse-transcribed into double-stranded cDNA with Actinomycin added during first-strand synthesis. The cDNA samples were fragmented, end-repaired and adenylated before ligation of TruSeq adapters. The adapters contain the index for multiplexing. Fragments containing TruSeq adapters on both ends were selectively enriched with PCR. The quality and quantity of the enriched libraries were validated using Qubit® (1.0) Fluorometer (Life Technologies, California, USA) and the Bioanalyzer 2100 (Agilent Technologies). The product is a smear with an average fragment size of approximately 360 bp. The libraries were normalized to 10nM in Tris-Cl 10 mM, pH8.5 with 0.1% Tween 20. The TruSeq SR Cluster Kit v4-cBot-HS (Illumina, Inc, California, USA) was used for cluster generation using 8 pM of pooled normalized libraries on the cBOT. Sequencing was performed on the Illumina HiSeq 4000 single end 125 bp using the TruSeq SBS Kit v4-HS (Illumina, Inc, California, USA). Reads were quality-checked with FastQC. For RNAseq data analysis, we used RSEM to perform RNAseq read alignment and expression estimation [62]. As reference we used the GRCm38 genome assembly and the corresponding gene annotations provided by Ensembl. We computed differential expression with the Bioconductor package DESeq2 [63]. A gene was considered as differentially expressed by applying a threshold of < 0.05 for the *p*-value and >0 for the |log2 ratio| (fold change). Additionally, we filtered away genes that had very low counts. Specifically, we did not consider a gene as expressed if it did not exceed in at least one condition an average read count of 10 in the samples. All clusterings and visualizations were performed with R/Bioconductor (R version 3.2). Raw RNA-seq data were deposited in NCBI Sequence Read Archive (SRA) under BioProject accession number PRJNA1260716.

Statistical analysis

Results are presented as the mean of replicas ± SEM. Unpaired Student's t-test was used for comparing two groups. Two-way ANOVA was used for the microglial sholl analysis. For survival curves of the in vivo experiments, all groups were compared by Log-rank (Mantel-Cox) test. *p*-values < 0.05 were considered statistically significant.

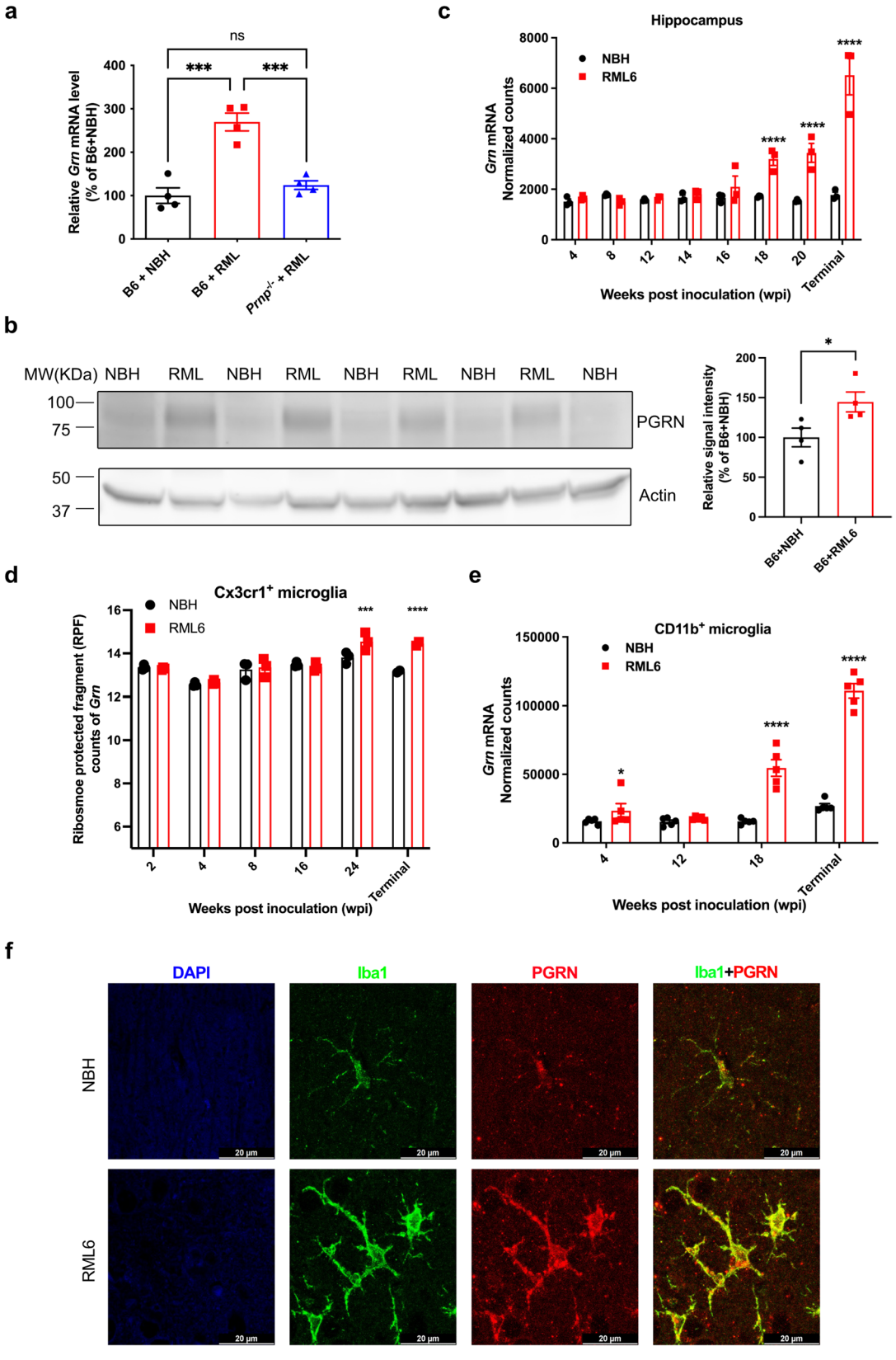

Fig. 1 (See legend on next page.)

(See figure on previous page.)

Fig. 1 Upregulation of PGRN expression in prion-infected mouse brains. (**a**) qRT-PCR for *Grn* mRNA from terminally sick RML6-infected C57BL/6J mice (B6 + RML) and age-matched NBH-inoculated C57BL/6J mice (B6 + NBH) and RML6-inoculated *Prnp*$^{-/-}$ mice (*Prnp*$^{-/-}$+RML) ($n = 4$). Relative expression was normalized to *Gapdh* expression and represented as percentage of average values in NBH-treated mice. (**b**) Left, Western blot for PGRN and Actin on brains collected from terminally sick RML6-infected C57BL/6J mice and age-matched NBH-inoculated C57BL/6J mice ($n = 4 \sim 5$). Right, densitometric quantification of the PGRN Western blot ($n = 4 \sim 5$). (**c**) RNA-Seq data of *Grn* expression in hippocampi at different time points after prion inoculation ($n = 3$). (**d**) Ribosomal profiling of *Grn* expression in CX3CR1-positive microglia at different time points after prion inoculation ($n = 3$, except $n = 2$ at terminal stage). (**e**) RNA-Seq data of *Grn* expression in sorted microglia (CD11b^{+}) at different time points after prion inoculation ($n = 5$). (**f**) Immunofluorescence staining of PGRN on brain sections from RML6- and NBH-inoculated mice. Scale bar: 20 µm. ns: $P > 0.05$; *: $P < 0.05$; ***: $P < 0.001$; ****: $P < 0.0001$

Results

Prion infection upregulates PGRN expression in mouse brain

To investigate whether the PGRN expression is altered by prion infection, we first performed quantitative reverse-transcription PCR (qRT-PCR) on forebrain mRNA isolated from terminally scrapie-sick wild-type (WT) C57BL/6J mice infected with the Rocky Mountain Laboratory strain of mouse-adapted scrapie prions (passage 6, therefore named RML6) (B6 + RML). Age-matched WT C57BL/6J mice inoculated with non-infectious brain homogenates (NBH) served as controls (B6 + NBH). We found that *Grn* mRNA was significantly increased in RML6 infected mouse forebrains (Fig. 1a). As an additional control, we included RML6-inoculated *Prnp*$^{-/-}$ mice (*Prnp*$^{-/-}$ +RML), which are resistant to prion infection and do not develop prion disease. These mice exhibited *Grn* mRNA levels similar to those in NBH-treated WT C57BL/6J mice (Fig. 1a), indicating that the upregulation of *Grn* mRNA is specifically associated with prion-induced pathology. Western blot analysis further confirmed that PGRN protein levels were significantly elevated in RML6-infected C57BL/6J mouse forebrains (Fig. 1b, full uncropped blot image in Suppl Fig. 1a, 1a').

Additionally, leveraging a time course RNA sequencing (RNA-Seq) study of hippocampal transcriptome in prion-infected mice [64], we compared the *Grn* expression in RML6 and NBH-inoculated C57BL/6J mouse hippocampi. We observed a significant increase in *Grn* mRNA levels in prion-infected mice from 18 weeks post-inoculation (wpi) until the terminal stage, compared to the NBH inoculated mice (Fig. 1c).

To identify the cell type responsible for the upregulation of *Grn* expression during prion infection, we analyzed data from cell-type-specific ribosomal profiling using CX3CR1-CreER, CamKIIa-Cre, and GFAP-Cre mice [65]. This analysis revealed that *Grn* expression was markedly upregulated in microglia at 24 wpi and the terminal stage (Fig. 1d), whereas no significant changes were observed in neurons or astrocytes (Suppl Fig. 2). To confirm that the increased *Grn* mRNA level reflected an absolute upregulation of *Grn* gene expression in microglia -rather than merely a consequence of prion-induced microglial proliferation [54]- we performed magnetic activated cell sorting (MACS) to isolate CD11b^{+} microglia from RML6-infected or NBH-treated C57BL/6J mouse brains. RNA-Seq analysis of these microglia confirmed that *Grn* mRNA levels were significantly elevated from 18 wpi until the terminal stage (Fig. 1e). Furthermore, immunostaining of brain sections from RML6 or NBH-inoculated mice demonstrated that the increased PGRN expression were predominantly localized to microglia (Fig. 1f).

Notably, a recent microarray analysis of sporadic Creutzfeldt-Jakob disease (sCJD) and non-neurological controls revealed that *GRN* transcription levels were significantly higher in sCJD brains [66]. Collectively, these findings indicate that *Grn* expression in the brain, particularly in microglia, is robustly upregulated by prion infection, suggesting that PGRN may play a role in prion pathogenesis and associated neuroinflammation.

Complete depletion, but not haploinsufficiency, of PGRN accelerates prion progression

To investigate whether PGRN deficiency influences prion pathogenesis, we intracerebrally inoculated 1.5-2-month-old *Grn*$^{-/-}$, *Grn*$^{+/-}$ and *Grn*$^{+/+}$ (WT) littermates with RML6 prions. The incubation time was defined as the interval between prion inoculation and the onset of terminal scrapie symptoms, at which point mice were euthanized. We found that haploinsufficiency of PGRN (*Grn*$^{+/-}$) did not affect prion progression, whereas complete depletion of PGRN (*Grn*$^{-/-}$) significantly accelerated the disease. *Grn*$^{-/-}$ mice exhibited significantly earlier onset of clinical symptoms and shorter incubation times compared to isogenic WT littermates (median survival: 166.5 days post inoculation (dpi) for *Grn*$^{-/-}$, $n = 18$, vs. 177 dpi for WT littermates, $n = 15$, $^{***}p = 0.0002$) (Fig. 2a). *Grn*$^{+/-}$ mice showed incubation times similar to WT littermates (median survival: 174 dpi, $n = 25$). Interestingly, there was no difference in the terminal clinical signs or intensity between different groups. These results indicate that complete PGRN deficiency, but not haploinsufficiency, accelerates prion progression, underscoring the neuroprotective role of PGRN in prion pathogenesis.

To evaluate the impact of PGRN deficiency on prion-induced neuropathology and astrogliosis, brains were collected from prion-infected *Grn*$^{-/-}$, *Grn*$^{+/-}$ and *Grn*$^{+/+}$ mice at the terminal stage (when mice were ~ 7–8 months old). Histological analysis revealed similar lesion patterns, visualized as vacuolation, across all groups, with slightly more vacuoles in the thalamus of *Grn*$^{-/-}$ mice ($n = 5 \sim 6$,

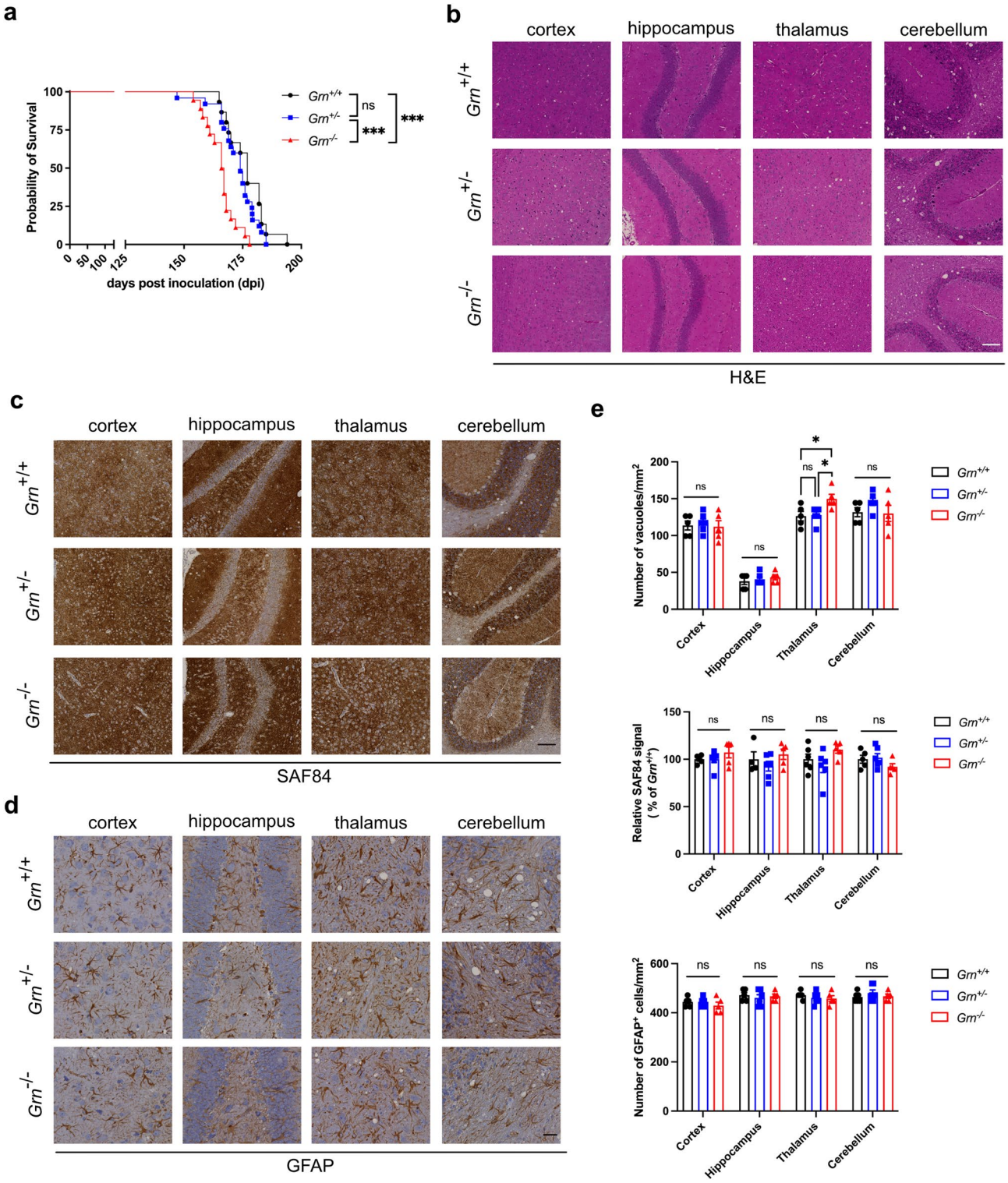

Fig. 2 PGRN deficiency accelerated prion progression. (**a**) Survival curves of RML6 infected *Grn*$^{-/-}$, *Grn*$^{+/-}$ and *Grn*$^{+/+}$ (WT) mice. The median survival of *Grn*$^{-/-}$ mice was 166.5 dpi ($n=18$) whereas that of *Grn*$^{+/+}$ (WT) females was 177 dpi ($n=15$). The median survival of *Grn*$^{+/-}$ mice was 174 dpi ($n=25$). (**b-d**) Representative histology of terminally sick mouse brains from *Grn*$^{-/-}$, *Grn*$^{+/-}$ and *Grn*$^{+/+}$ (WT) littermates stained for Hematoxylin/Eosin (H&E) (**b**), SAF84 (**c**) and GFAP (**d**). Scale bar: 100 µm in (**b**) and (**c**), 25 µm in (**d**). (**e**): Quantitation of the vacuoles (upper panel), SAF84 signal (middle panel) and GFAP^{+} cells (lower panel). $n=5\sim6$ for each group and each brain region. ns: $P>0.05$; *: $P<0.05$; ***: $P<0.001$

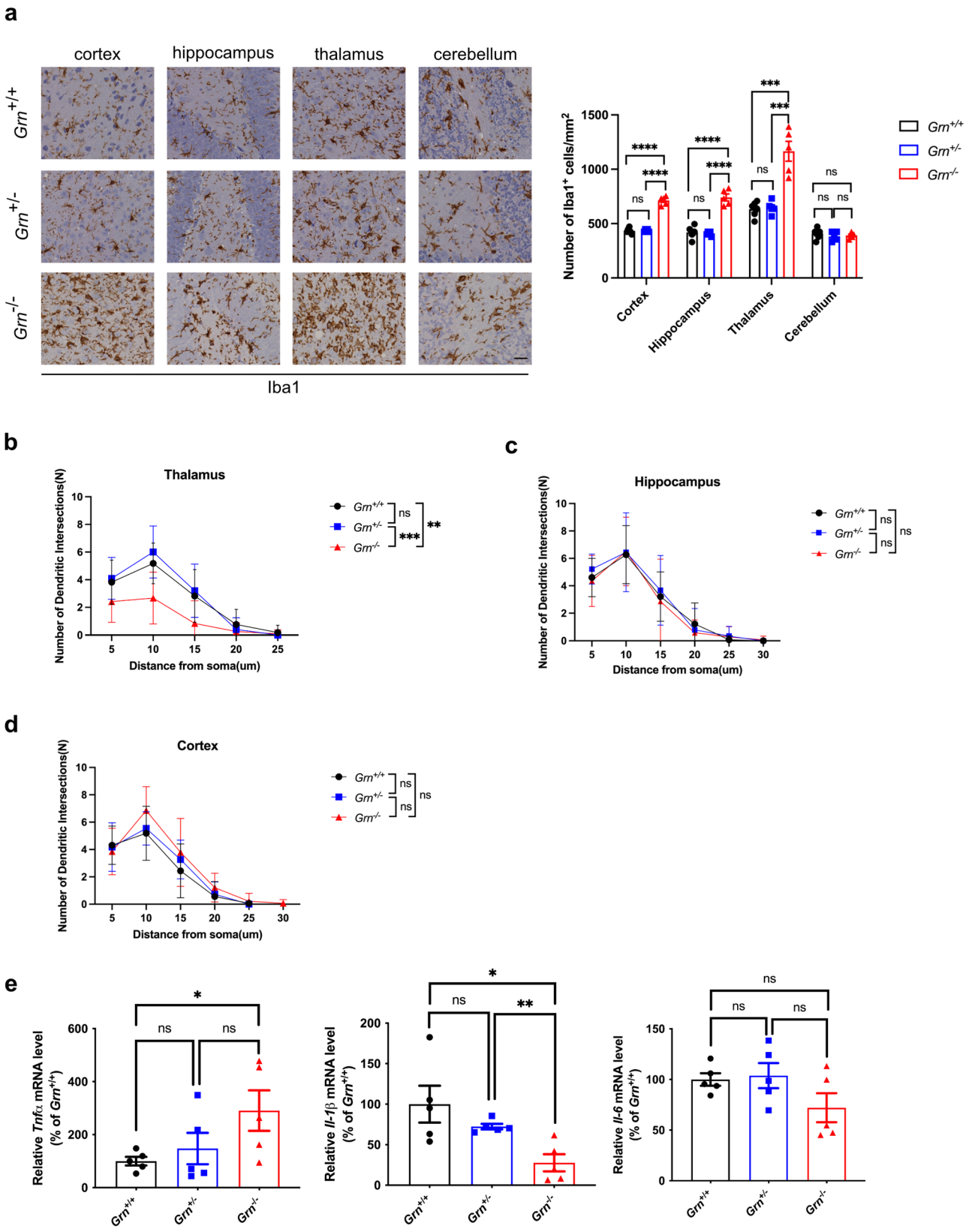

Fig. 3 (See legend on next page.)

(See figure on previous page.)

Fig. 3 Augmented microglial activation and altered cytokine profiles in prion-infected *Grn*$^{-/-}$ mice. (**a**) Left, representative histology of Iba1 immunohistochemistry of various brain regions from RML6-infected *Grn*$^{-/-}$, *Grn*$^{+/-}$ and *Grn*$^{+/+}$ (WT) littermates at terminal stage. Scale bar: 25 μm. Right, quantification of Iba1 staining. $n = 5 \sim 6$ for each group and each brain region. (**b-d**) Sholl analysis of Iba^{+} microglia at cortex (**b**), hippocampus (**c**) and thalamus (**d**) of *Grn*$^{-/-}$, *Grn*$^{+/-}$ and *Grn*$^{+/+}$ (WT) mice at terminal stage. $n = 5 \sim 6$ mice per group, 5–6 microglia/region/mouse were analyzed. (**e**) qRT-PCR of *Tnfa*, *Il-1β* and *Il-6* mRNA in RML6-infected *Grn*$^{-/-}$, *Grn*$^{+/-}$ and *Grn*$^{+/+}$ (WT) brains at terminal stage. $n = 5$. ns: $P > 0.05$; *: $P < 0.05$; **: $P < 0.01$; ***: $P < 0.001$; ****: $P < 0.0001$

Fig. 2b, e). PrP^{Sc} deposition, assessed by SAF84 staining, was also comparable in different brain regions at the terminal stage ($n = 5 \sim 6$, Fig. 2c, e). GFAP (glial fibrillar acidic protein) staining showed no significant differences in reactive astrocytes among the three groups ($n = 5 \sim 6$, $401 \sim 472$ cells/mm^2, Fig. 2d, e), suggesting that astrogliosis at the terminal stage is not influenced by PGRN deficiency. H&E and SAF84 staining on NBH-inoculated *Grn*$^{-/-}$ and *Grn*$^{+/+}$ mice at the same age ($7 \sim 8$ months old) demonstrated no vacuolation or PrP^{Sc} deposition in the brains (Suppl Fig. 3a, b), GFAP staining revealed similar astrocyte numbers in NBH-inoculated *Grn*$^{-/-}$ and *Grn*$^{+/+}$ mouse brains (Suppl Fig. 3c).

It has been previously reported that *Grn*$^{-/-}$ mice developed TDP-43 proteinopathy by 24 months of age [42]. However, we did not detect obvious TDP-43 pathology in the brains of prion-infected *Grn*$^{+/-}$ or *Grn*$^{-/-}$ mice at the terminal stage (data not shown), indicating that prion infection does not accelerate TDP-43 proteinopathy induced by PGRN insufficiency.

Augmented microglial activation in prion-infected Grn$^{-/-}$ mice

Given that PGRN has been shown to regulate microglial activation in various pathological contexts [34, 37] and during aging [40, 46], we investigated the effect of PGRN deficiency on prion-induced microglial activation. Iba1 (ionized calcium-binding adaptor molecule 1) staining on brain sections from terminally sick *Grn*$^{-/-}$, *Grn*$^{+/-}$ and *Grn*$^{+/+}$ mice revealed significantly augmented microglial activation in the cortex, hippocampus and thalamus of *Grn*$^{-/-}$ mice compared to *Grn*$^{+/-}$ and *Grn*$^{+/+}$ littermates ($n = 5 \sim 6$, Fig. 3a). Consistent with previous observations in aging brains, the augmentation was most pronounced in thalamus. Interestingly, microglial activation in the cerebellum was similar across all genotypes, suggesting that the enhanced microglial activation is brain region-specific (Fig. 3a). Iba-1 staining on NBH-inoculated *Grn*$^{-/-}$ and *Grn*$^{+/+}$ mouse brains revealed similar microglia numbers (Suppl Fig. 3d). Although 7-month-old *Grn*$^{-/-}$ mice have been reported to exhibit slightly increased microglial activation compared to age-matched *Grn*$^{+/-}$ and *Grn*$^{+/+}$ mice [38], prion infection drastically exacerbated this activation. Morphologically, *Grn*$^{-/-}$ microglia in thalamus displayed an ameboid shape with enlarged cell bodies and shortened processes. Sholl analysis of Iba1^{+} microglial morphology confirmed that thalamic *Grn*$^{-/-}$ microglia have significant fewer processes (Fig. 3b). In contrast, while microglial proliferation was enhanced in hippocampus and cortex of *Grn*$^{-/-}$ mice, their morphology remained similar to that of *Grn*$^{+/+}$ and *Grn*$^{+/-}$ microglia (Fig. 3c-d).

Cytokine analysis revealed that TNFα were significantly elevated in *Grn*$^{-/-}$ mouse brains compared to *Grn*$^{+/-}$ and *Grn*$^{+/+}$littermates, whereas IL-1β and IL-6 was downregulated or showed a decreasing trend (Fig. 3e). These findings suggest that complete PGRN deficiency enhances prion-induced microglial activation and alters cytokine profiles, indicating that PGRN acts as a brake on prion-induced microglial activation.

Enhanced prion clearance in Grn$^{-/-}$ mice at 120 Dpi but not at 150 Dpi

To further explore the impact of PGRN deficiency on prion-induced microglial activation, we collected brains from prion-infected *Grn*$^{-/-}$, *Grn*$^{+/-}$ and *Grn*$^{+/+}$ mice at 120 dpi (when mice were ~6 months old), when mice began developing scrapie symptoms. Iba1 staining revealed significantly enhanced microglial activation in *Grn*$^{-/-}$ mouse brains (primarily thalami) compared to *Grn*$^{+/-}$ and *Grn*$^{+/+}$ littermates (Fig. 4a, upper panel; Suppl Fig. 4a). Interestingly, histological and Western blot analysis of forebrains showed that PrP^{Sc} deposition at this stage was significantly reduced in *Grn*$^{-/-}$ mice (Fig. 4b upper panel, 4c; Suppl Fig. 4b; full uncropped blot image in Suppl Fig. 1b), although the total PrP are similar between different groups (Suppl Fig. 4c). These results suggest that microglia at this stage exhibit a phagocytic phenotype, and the enhanced microglial activation enables more efficient prion clearance. Since vacuolation induced by prion infection was minimal at this stage, no differences were observed between genotypes (Suppl Fig. 4d). Similarly, GFAP staining revealed no significant differences in astrogliosis among different genotypes at this stage (Suppl Fig. 4e).

At 150 dpi (when mice were ~7 months old), when mice were severely sick and nearing the terminal stage, microglial activation remained significantly enhanced in *Grn*$^{-/-}$ mouse thalami compared to *Grn*$^{+/-}$ and *Grn*$^{+/+}$ littermates (Fig. 4a, lower panel; Suppl Fig. 4a). However, forebrain PrP^{Sc} deposition in *Grn*$^{-/-}$ mice at this stage was similar to that of *Grn*$^{+/-}$ and *Grn*$^{+/+}$ mice (Fig. 4b lower panel, 4d; Suppl Fig. 4b; full uncropped blot image in Suppl Fig. 1c). This suggests that excessive microglial activation in *Grn*$^{-/-}$ mice at 150 dpi was less effective in clearing prions compared to the 120 dpi stage. These

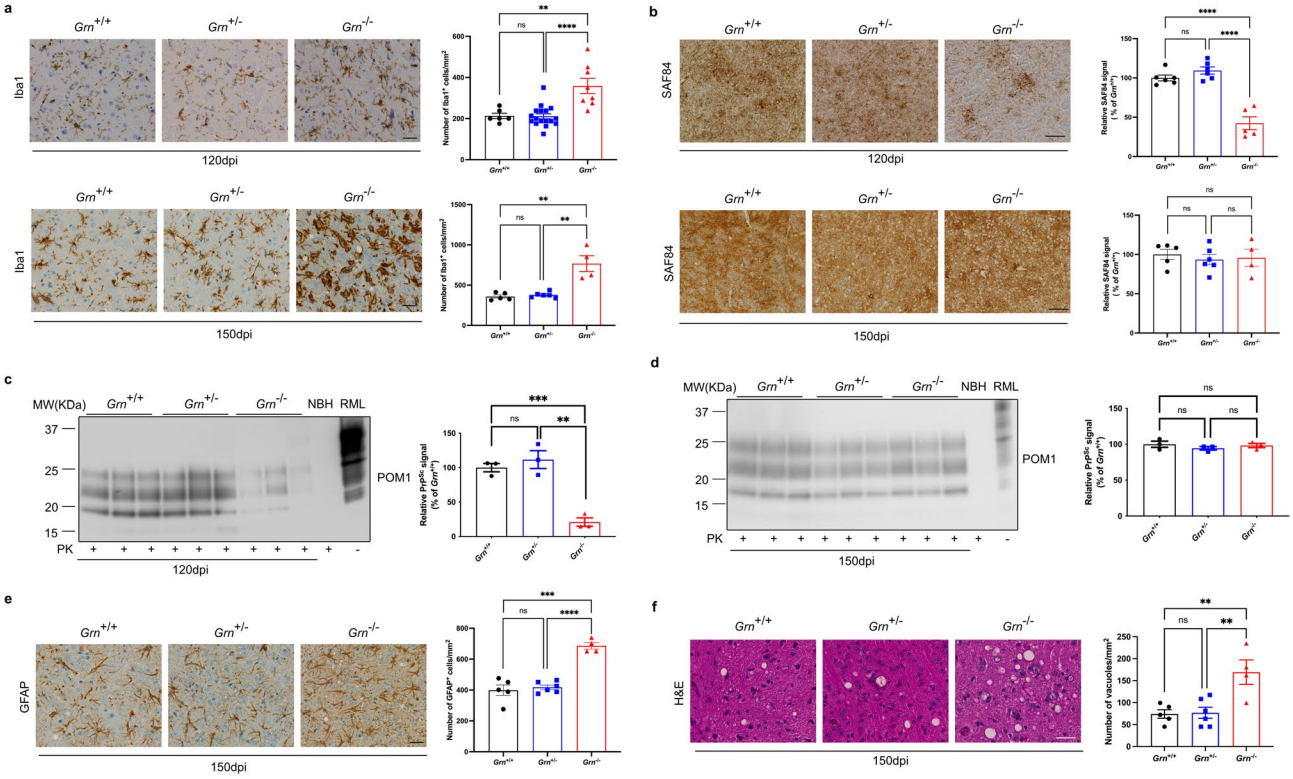

Fig. 4 Enhanced prion clearance in *Grn*$^{-/-}$ mice at 120dpi, but not at 150dpi. (**a**) Upper panel: left, representative histology of Iba1 immunohistochemistry of thalamus from RML6-infected *Grn*$^{-/-}$, *Grn*$^{+/-}$ and *Grn*$^{+/+}$ (WT) littermates at 120 dpi. Scale bar: 25 μm. Right, quantification of Iba1^{+} cells at thalamus. $n = 6 \sim 17$. Lower panel: left, representative histology of Iba1 immunohistochemistry of thalamus from RML6-infected *Grn*$^{-/-}$, *Grn*$^{+/-}$ and *Grn*$^{+/+}$ (WT) littermates at 150 dpi. Scale bar: 25 μm. Right, quantification of Iba1^{+} cells at thalamus. $n = 4 \sim 6$. (**b**) Upper panel: left, representative histology of SAF48 immunohistochemistry of thalamus from RML6-infected *Grn*$^{-/-}$, *Grn*$^{+/-}$ and *Grn*$^{+/+}$ (WT) littermates at 120 dpi. Scale bars: 100 μm. Right, quantification of SAF84 staining. $n = 5 \sim 6$. Lower panel: left, representative histology of SAF48 immunohistochemistry of thalamus from RML6-infected *Grn*$^{-/-}$, *Grn*$^{+/-}$ and *Grn*$^{+/+}$ (WT) littermates at 150 dpi. Scale bars: 100 μm. Right, quantification of SAF84 staining. $n = 4 \sim 6$. (**c**) Left, PrP^{Sc} Western blot of homogenates prepared from RML6-infected *Grn*$^{-/-}$, *Grn*$^{+/-}$ and *Grn*$^{+/+}$ (WT) mouse brains at 120 dpi. NBH control was WT brain homogenates inoculated with NBH at the same age. Samples were digested with PK as indicated and detected with POM1. Right, densitometric quantification of the PrP^{Sc} Western blot. $n = 3$. (**d**) Left, PrP^{Sc} Western blot of homogenates prepared from RML6-infected *Grn*$^{-/-}$, *Grn*$^{+/-}$ and *Grn*$^{+/+}$ (WT) mouse brains at 150 dpi. NBH control was WT brain homogenates inoculated with NBH at the same age. Samples were digested with PK as indicated and detected with POM1. Right, densitometric quantification of the PrP^{Sc} Western blot. $n = 3$. (**e**) Left, representative histology of GFAP immunohistochemistry of thalamus from RML6-infected *Grn*$^{-/-}$, *Grn*$^{+/-}$ and *Grn*$^{+/+}$ (WT) littermates at 150 dpi. Scale bar:25 μm. Right: quantification of GFAP^{+} cells at thalamus. $n = 4 \sim 6$. (**f**) Left, representative histology of H&E staining of thalamus from RML6-infected *Grn*$^{-/-}$, *Grn*$^{+/-}$ and *Grn*$^{+/+}$ (WT) littermates at 150 dpi. Scale bars: 100 μm. Right: quantification of vacuoles at thalamus. $n = 4 \sim 6$. ns: $P > 0.05$; **: $P < 0.01$; ***: $P < 0.001$; ****: $P < 0.0001$

findings imply that prion-induced microglial activation occurs in a stepwise manner: at 120 dpi, the activated microglia exhibit a phagocytic phenotype, while at 150 dpi, they transition to a less efficient state with reduced prion clearance capacity.

Interestingly, GFAP staining revealed enhanced astrogliosis in *Grn*$^{-/-}$ thalami at 150 dpi (Fig. 4e), consistent with recent reports that PGRN deficiency leads to aberrant astrocytic phenotype promoting synaptic degeneration [67]. Importantly, *Grn*$^{-/-}$ thalami exhibited more severe vacuolation at this stage compared to *Grn*$^{+/-}$ and *Grn*$^{+/+}$ littermates (Fig. 4f). These results indicate that complete deficiency of PGRN exacerbates prion pathology as the disease progresses, correlating with the shortened incubation time observed in *Grn*$^{-/-}$ mice.

Lack of progranulin in prion-infected mice results in abnormal immune response and altered microglial States

To investigate how complete PGRN deficiency augments microglial activation and accelerates prion progression, we isolated microglia (CD11b^{+}) from prion-infected *Grn*$^{-/-}$, *Grn*$^{+/-}$and *Grn*$^{+/+}$ (WT) mouse forebrains at 150 dpi (~ 7 months old) using MACS and performed whole-transcriptome analyses by RNA-seq. The purities of sorted microglia were analyzed by flow cytometry and >90% cells were positive for CD11b (data not shown), consistent with previous reports [68]. The multidimensional scaling (MDS) plot showed that *Grn*$^{+/-}$ (Het) and *Grn*$^{+/+}$ (WT) microglial replicates clustered closely, whereas *Grn*$^{-/-}$ (KO) microglia exhibited a distinct transcriptomic profile (Suppl Fig. 5a). These results suggest that haploinsufficiency of PGRN has a modest effect on

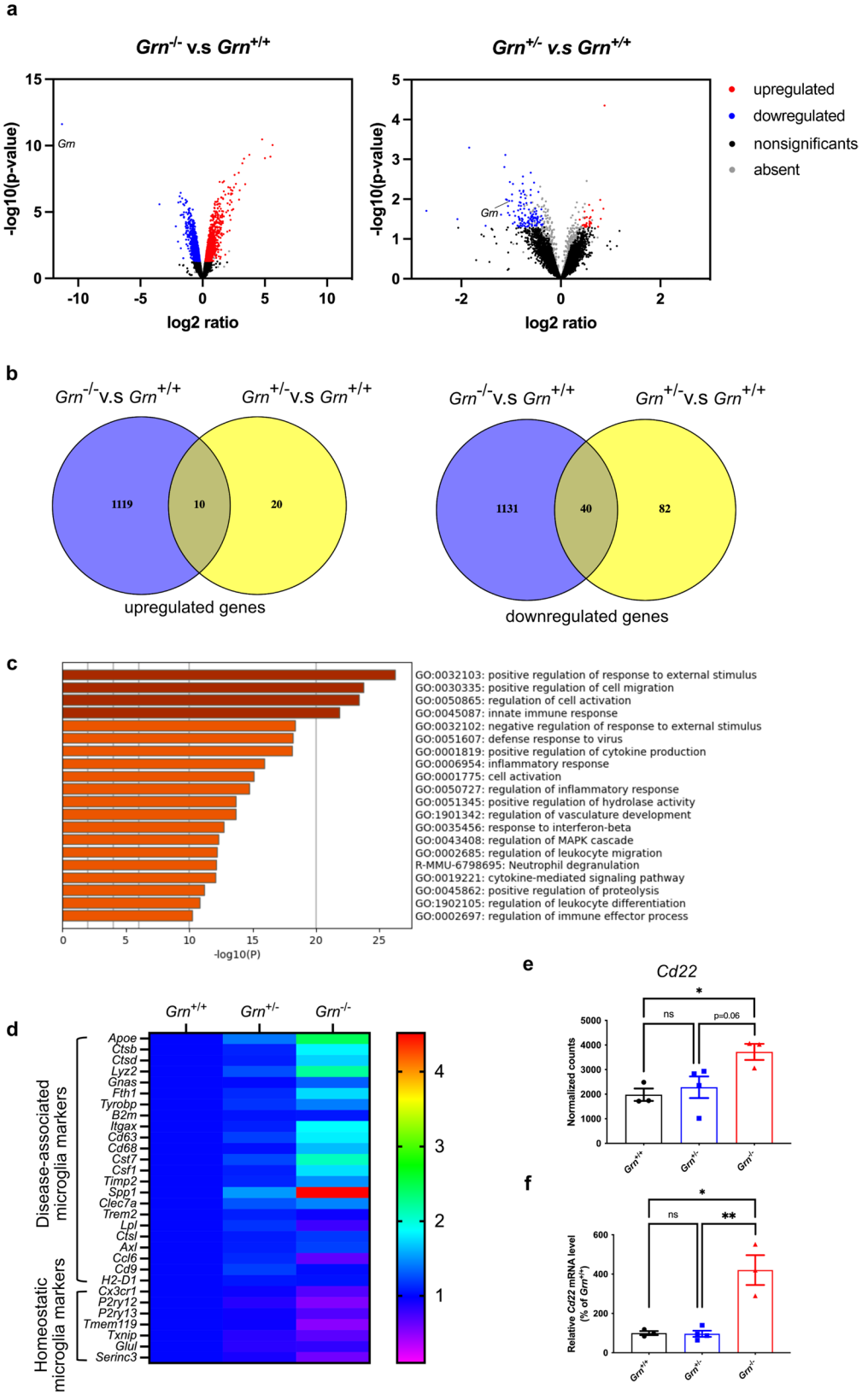

Fig. 5 (See legend on next page.)

(See figure on previous page.)

Fig. 5 PGRN deficiency shifted microglia from homeostatic to disease-associated states in prion-infected mouse brains. (**a**) Volcano plots of RNAseq data for microglia (CD11b$^+$) from prion-infected *Grn*$^{-/-}$, *Grn*$^{+/-}$ and *Grn*$^{+/+}$ (WT) mouse brains at 150 dpi. Left, *Grn*$^{-/-}$ v.s *Grn*$^{+/+}$. Right, *Grn*$^{+/-}$ v.s *Grn*$^{+/+}$. Upregulated (red dots) and downregulated (blue dots) are genes that show fold change (fc) > 1 or <-1 with $P < 0.05$. $P > 0.05$: nonsignificant. Genes that are not detected: absent. $n = 3$ for *Grn*$^{-/-}$ and *Grn*$^{+/+}$, $n = 4$ for *Grn*$^{+/-}$. (**b**) Venn diagram of overlapping differentially expressed genes (DEGs) between *Grn*$^{-/-}$ v.s *Grn*$^{+/+}$ and *Grn*$^{+/-}$ vs. *Grn*$^{+/+}$. Left: significantly upregulated genes; Right: significantly downregulated genes. (**c**) GO analysis of DEGs between *Grn*$^{-/-}$ and *Grn*$^{+/+}$. (**d**) Heat map of disease-associated markers and homeostatic markers of RNAseq data for microglia (CD11b$^+$) from prion-infected *Grn*$^{-/-}$ mouse brains at 150 dpi. (**e**, **f**) Read counts and qRT-PCR of phagocytosis negative regulator *Cd22* in CD11b$^+$ microglia from prion-infected *Grn*$^{-/-}$, *Grn*$^{+/-}$ and *Grn*$^{+/+}$ (WT) mouse brains at 150 dpi. $n = 3$ for *Grn*$^{-/-}$ and *Grn*$^{+/+}$, $n = 4$ for *Grn*$^{+/-}$. ns: $P > 0.05$; *: $P < 0.05$

microglial transcriptomes, while complete deficiency of PGRN leads to profound alterations in microglial gene expression.

We compared the gene expression changes between *Grn*$^{-/-}$, *Grn*$^{+/-}$ and *Grn*$^{+/+}$ microglia (Suppl Table 1). *Grn*$^{-/-}$ microglia showed 2,300 differentially expressed genes (DEGs) (1,129 upregulated, 1,171 downregulated) compared to *Grn*$^{+/+}$ microglia ($p < 0.05$), whereas *Grn*$^{+/-}$ microglia exhibited only 152 DEGs (30 upregulated, 122 downregulated) relative to *Grn*$^{+/+}$ microglia (Fig. 5a). Among these, 10 upregulated and 40 downregulated (including *Grn* itself) DEGs overlapped between *Grn*$^{-/-}$ v.s *Grn*$^{+/+}$ and *Grn*$^{+/-}$ v.s *Grn*$^{+/+}$ microglia (Fig. 5b). Gene enrichment analysis of the 2,300 DEGs in *Grn*$^{-/-}$ microglia by Metascape online tool (http://metascape.org/) revealed significant involvement in pathways related to positive and negative regulation of response to external stimulus, positive regulation of cell migration, regulation of cell activation and innate immune response (Fig. 5c). These findings align with previous studies demonstrating abnormal immune responses caused by PGRN deficiency.

Interestingly, while PGRN deficiency alone showed moderate changes (45 DEGs) in microglial gene expression at 7 months of age in untreated mice revealed by single-nucleus RNA sequencing (snRNA-seq) [42], prion-infected *Grn*$^{-/-}$ mice at the same age exhibited more profound transcriptional alterations in microglia. There was an overlap of 28 DEGs between *Grn*$^{-/-}$ microglia isolated from prion-infected mice or untreated mice at 7 months old (Suppl Fig. 5b, overlapping genes are highlighted in yellow and orange in suppl Table 1). Notably, 19 of the 21 consistently dysregulated genes in *Grn*$^{-/-}$ microglia across different ages (7 months, 12 months and 19 months of age) were also differentially expressed in *Grn*$^{-/-}$ microglia from prion-infected mice (Suppl Fig. 5c, overlapping genes are highlighted in orange in suppl Table 1). These results suggest synergistic effects between prion infection and PGRN deficiency.

Although the transcriptional profiles of aged *Grn*$^{-/-}$ microglia diverge significantly from those of disease-associated microglia (DAM) [42, 69], microglia from prion-infected *Grn*$^{-/-}$ mice showed increased expression of most DAM markers (e.g. *Apoe*, *Ctsb*, *Ctsd*, *Itgax*, *Cd63* and *Cd68*), and decreased expression of homeostatic markers (e.g. *Cx3cr1*, *P2ry12*, *P2ry13*, *Tmem119*) (Fig. 5d). These results suggest that complete PGRN deficiency accelerates the transition of microglia from a homeostatic state to a disease-associated phenotype in prion-infected mice. Importantly, *Grn*$^{-/-}$ microglia at 150 dpi exhibited significantly upregulated expression of CD22 (Fig. 5e, f), a recently identified negative regulator of microglia phagocytosis [70, 71]. This may explain the impaired prion clearance observed at this stage. Notably, we observed that prion infection alone significantly upregulated CD22 expression in both bulk brain tissue and isolated microglial after 18 wpi (Suppl Fig. 5d, e). Moreover, CD22 levels were already elevated in noninfected *Grn*$^{-/-}$ brains (7 months old) and *Grn*$^{-/-}$ microglia compared to wild-type controls (Suppl Fig. 5f, g). Together, these findings suggest a synergistic effect of prion infection and PGRN deficiency on CD22 upregulation at 150 dpi.

PGRN deficiency in prion-infected mice results in aggravated complement activation

Innate immune response emerged as one of the top dysregulated pathways in prion-infected *Grn*$^{-/-}$ mice. Previous studies have reported aberrant activation of complement cascade in *Grn*$^{-/-}$ mice, leading to excessive synaptic pruning, TDP-43 neuropathology, and neurotoxicity [40, 42]. To determine whether complement activation contributes to the accelerated prion progression in *Grn*$^{-/-}$ mice, we first assessed complement cascade activation in prion-infected mouse brains. qRT-PCR and WB analysis revealed that *C1qa* and *C3* mRNA levels were upregulated in RML6 infected mice (Fig. 6a). Similarly, the protein levels of C1qa and C3 cleavage products iC3b were increased in prion-infected brains (Fig. 6b, full uncropped blots images in Suppl Fig. 1d-e). Temporal RNA-seq analysis confirmed upregulation of C1qa and C3 in both bulk tissue and microglia after 18 wpi (Suppl Fig. 6a-d).

We then evaluated complement components in *Grn*$^{-/-}$, *Grn*$^{+/-}$ and *Grn*$^{+/+}$ mouse forebrains infected with RML6 at 120dpi and 150dpi. While C1qa and C3 levels were unchanged in *Grn*$^{-/-}$ mice at 120dpi, both were significantly upregulated in *Grn*$^{-/-}$ mice at 150dpi (Fig. 6c-f, full uncropped blots images in Suppl Fig. 1f-i). This aggravated complement activation in *Grn*$^{-/-}$ mice at 150dpi may partially explain the exacerbated neuronal lesion and accelerated prion progression observed in these mice. Interestingly, RNA-seq did not find significant increase of C1qa transcripts in *Grn*$^{-/-}$ microglia (Suppl Table 1),

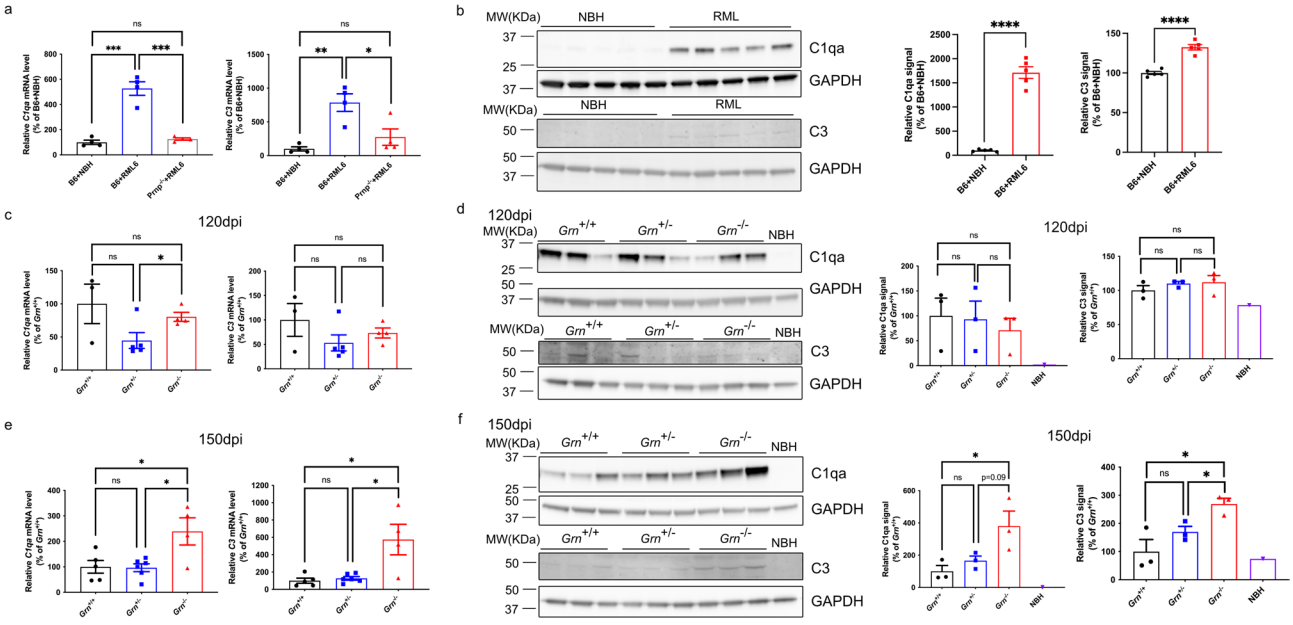

Fig. 6 Aggravated complement activation in prion-infected *Grn*$^{-/-}$ mouse brains. (**a**) qRT-PCR of *C1qa* (left) and *C3* (right) mRNA in prion-infected C57BL/6J mouse brains (B6 + RML). $n = 4$ (**b**) Left, Western blot of C1qa and C3 in prion-infected C57BL/6J mouse brains. Right, densitometric quantification of the C1qa and C3 Western blot. $n = 5$. (**c**) qRT-PCR of C1qa and C3 in prion-infected *Grn*$^{-/-}$, *Grn*$^{+/-}$ and *Grn*$^{+/+}$ (WT) mouse brains at 120 dpi. $n = 3 \sim 5$. (**d**) Left, Western blot of C1qa and C3 in prion-infected *Grn*$^{-/-}$, *Grn*$^{+/-}$ and *Grn*$^{+/+}$ (WT) mouse brains at 120 dpi. NBH control was WT brain homogenates inoculated with NBH at the same age (B6 + NBH). Right, densitometric quantification of the C1qa and C3 Western blot. $n = 3$. (**e**) qRT-PCR of C1qa and C3 in prion-infected *Grn*$^{-/-}$, *Grn*$^{+/-}$ and *Grn*$^{+/+}$ (WT) mouse brains at 150 dpi. $n = 4 \sim 5$. (**f**) Left, Western blot of C1qa and C3 in prion-infected *Grn*$^{-/-}$, *Grn*$^{+/-}$ and *Grn*$^{+/+}$ (WT) mouse brains at 150 dpi. NBH control was WT brain homogenates inoculated with NBH at the same age. Right, densitometric quantification of the C1qa and C3 Western blot. $n = 3$. ns: $P > 0.05$; *: $P < 0.05$; **: $P < 0.01$; ***: $P < 0.001$; ****: $P < 0.0001$

suggesting that greater microglial numbers and/or other cell types may contribute to the increased complement activation. Although depletion of C1qa or C3 alone does not alter prion progression following intracerebral infection [72], further studies are needed to determine whether ablation or antagonism of these complement components could mitigate prion acceleration induced by PGRN-deficiency.

Impaired autophagosome functions have been reported in aged *Grn*$^{-/-}$ mice. To investigate whether *Grn* deficiency exacerbates autophagosome dysfunction after prion infection, we performed Western blots analysis of LC3B and P62. However, no significant changes in these markers were observed in prion-infected *Grn*$^{-/-}$, *Grn*$^{+/-}$ and *Grn*$^{+/+}$ mice (Suppl Fig. 6e, f), suggesting that impaired autophagosome function is not responsible for the accelerated prion progression in *Grn*$^{-/-}$ mice.

Microglia-specific depletion of PGRN does not alter prion pathogenesis

Given that PGRN is primarily upregulated in microglia upon prion infection and PGRN deficiency leads to augmented microglial activation, we investigated whether microglia-specific deletion of *Grn* affects prion pathogenesis. We generated CX3CR1-CreERT;*Grn*$^{fl/fl}$ mice and treated them with Tamoxifen (Tx) for 4 weeks. RT-qPCR and ELISA confirmed significant reduction of *Grn* mRNA and PGRN protein levels in CX3CR1-CreERT;*Grn*$^{fl/fl}$ mice compared to Tx-treated *Grn*$^{fl/fl}$ control mice (Fig. 7a, b).

To assess the impact of microglia-specific PGRN depletion on prion pathogenesis, CX3CR1-CreERTx*Grn*$^{fl/fl}$ and *Grn*$^{fl/fl}$ mice were fed with tamoxifen diet (diet containing tamoxifen citrate 400 ppm, +Tx) for 4 weeks, followed by a normal diet for 2 weeks, before intracerebral inoculation with RML6. Control groups without tamoxifen diet feeding (-Tx) were also inoculated. Unexpectedly, prion progression was similar between CX3CR1-CreERT;*Grn*$^{fl/fl}$ and *Grn*$^{fl/fl}$ mice, regardless of tamoxifen treatment (median survival: 170 dpi for *Grn*$^{fl/fl}$ mice + Tx ($n = 25$), 170 dpi for CX3CR1-CreERT;*Grn*$^{fl/fl}$ +Tx ($n = 25$), 168 dpi for *Grn*$^{fl/fl}$ mice -Tx ($n = 24$), 173.5 dpi for CX3CR1-CreERT;*Grn*$^{fl/fl}$ -Tx ($n = 24$), $p = 0.62$) (Fig. 7c). Histological analysis also revealed no differences in lesion pattern, PrP^{Sc} deposition, astrogliosis, or microglial activation between CX3CR1-CreERT;*Grn*$^{fl/fl}$ and *Grn*$^{fl/fl}$ mice (Fig. 7d-g). Complement activation and CD22 expression were comparable between CX3CR1-CreERT;*Grn*$^{fl/fl}$ and *Grn*$^{fl/fl}$ mice (Suppl Fig. 7a, b, c).

These observations suggest that, unlike complete PGRN ablation, microglia-specific depletion of PGRN

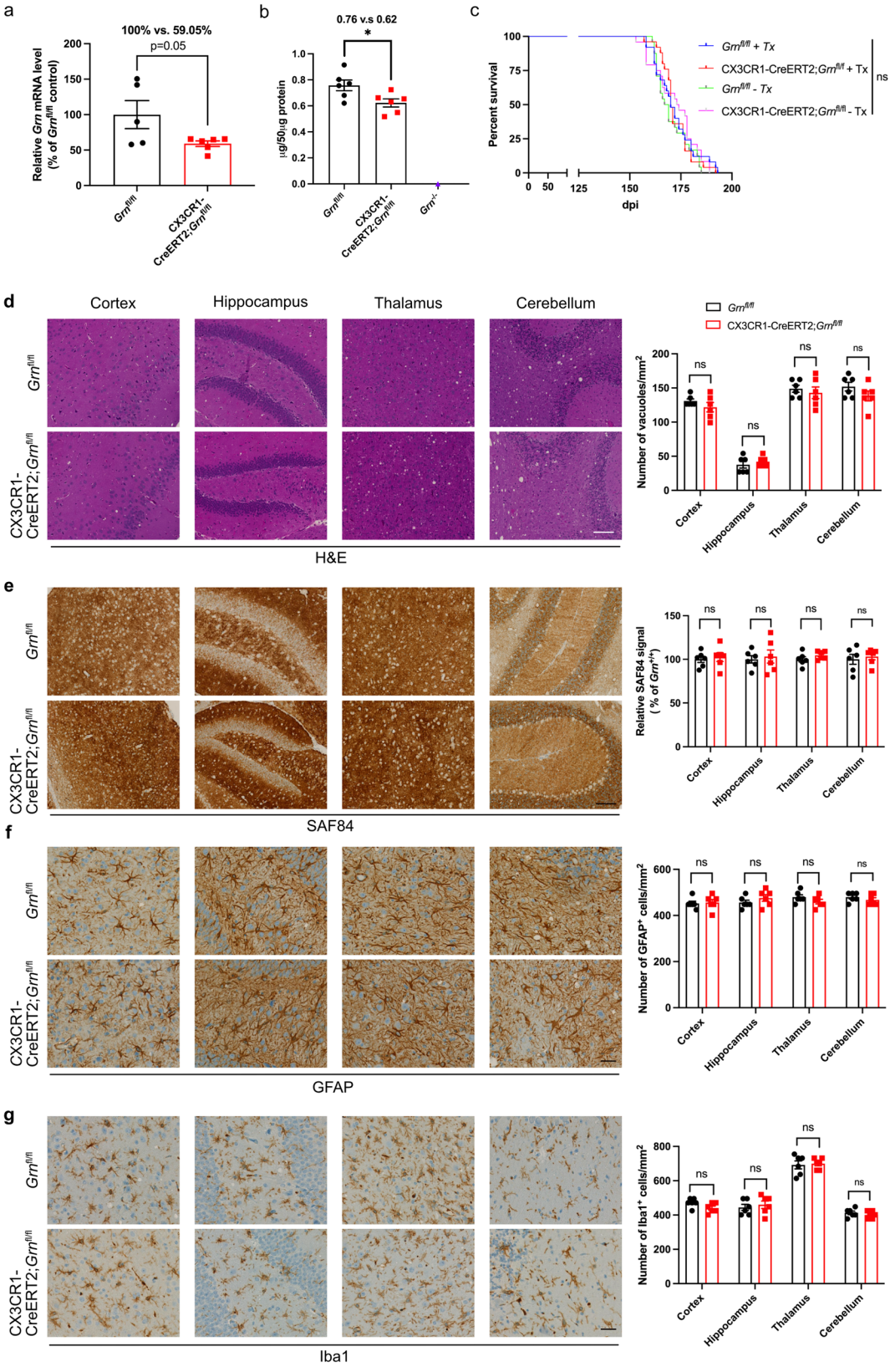

Fig. 7 (See legend on next page.)

(See figure on previous page.)

Fig. 7 Microglia specific *Grn* depletion did not alter prion pathogenesis. (**a**) qRT-PCR for *Grn* mRNA and (**b**) ELISA for PGRN levels in tamoxifen-treated CX3CR1-CreERT;$Grn^{fl/fl}$ and $Grn^{fl/fl}$ mouse brains. $n = 5 \sim 6$. (**c**) Survival curves of RML6-infected CX3CR1-CreERT;$Grn^{fl/fl}$ and $Grn^{fl/fl}$ mice untreated or treated with Tamoxifen. The median survival of $Grn^{fl/fl}$+Tx mice was 172 dpi ($n = 25$), CX3CR1-CreERT;$Grn^{fl/fl}$+Tx mice was 170.5 dpi ($n = 25$), $Grn^{fl/fl}$-Tx mice was 166 dpi ($n = 24$), CX3CR1-CreERT;$Grn^{fl/fl}$-Tx mice was 174dpi ($n = 24$). There was no significant difference between the groups. (**d-g**) Left, representative histology of cortex (**d**), hippocampus (**e**), thalamus (**f**) and cerebellum (**g**) of RML6-infected CX3CR1-CreERT;$Grn^{fl/fl}$ and $Grn^{fl/fl}$ mice treated with Tamoxifen. Scale bar: 100 μm in (**d**) and (**e**), 25 μm in (**f**) and (**g**). Right, quantification of vacuoles, SAF84 signals, $GFAP^+$ cells and Iba^+ cells at various brain regions. $n = 6$. ns: $P > 0.05$; *: $P < 0.05$

does not alter prion progression. This indicates that the augmented microglial activation observed in prion-infected $Grn^{-/-}$ mice is not cell-autonomous. Instead, PGRN expressed and released by other cell types, such as neurons, may regulate prion-induced microglial activation in a non-cell-autonomous manner. The crosstalk between microglia and other neural cells in prion pathogenesis warrants further investigation. Additionally, residual PGRN taken up by microglia from other cells or incomplete microglial depletion of *Grn* by Cx3cr1-CreERT-mediated recombination indicated by PGRN staining may mitigate the effects of microglia-specific *Grn* deficiency (Suppl Fig. 7d).

Discussion

The mechanisms by which PGRN deficiency leads to neurodegeneration are a subject of intense investigation. Our study demonstrates that PGRN expression in microglia is upregulated in response to prion infection. Complete depletion of *Grn*, but not haploinsufficiency, accelerates prion progression. PGRN ablation enhances prion-induced microglial activation, with microglia exhibiting increased phagocytic capacity at 120 dpi but losing this capability by 150 dpi, suggesting a phenotypic transition during this period. Both prion infection and PGRN-deficiency independently promote microglial activation, the augmented microglial response observed in prion-infected $Grn^{-/-}$ mice likely reflects a synergistic interaction between these two factors. Importantly, PGRN deficiency results in augmented complement cascade activation at 150 dpi, which may contribute to the accelerated prion disease progression. These findings highlight a neuroprotective role for PGRN in prion pathogenesis and expand our understanding of PGRN's functions in neurodegenerative diseases.

Most, if not all, pathological *GRN* mutations or polymorphisms result in reduced PGRN levels due to premature stop codons or mRNA decay. Consequently, plasma and/or cerebrospinal fluid (CSF) PGRN levels serve as important diagnostic biomarkers for *GRN*-related FTLD. Indeed, low PGRN levels reliably predict *GRN* mutations in FTLD patients [73–78]. Notably, reduced CSF PGRN levels have also been observed in FTLD patients without *GRN* mutations [79]. Interestingly, while AD patients carrying *GRN* mutations exhibit lower PGRN levels [17, 20, 23, 80], PGRN levels are elevated in other AD patients [81, 82]. In mouse models of AD, PGRN levels increase in microglia clustering around amyloid plaques [83]. However, in other AD models, PGRN levels decrease in the early disease stages but increase at later stages [50]. These findings suggest that PGRN expression varies dynamically across different neurodegenerative diseases, depending on the context and disease stage. Interestingly, our study observed an upregulation of microglial PGRN at the late stage of prion infection, suggesting a potential role of PGRN in prion-induced neuroinflammation and neurodegeneration.

The effect of PGRN deficiency on prion disease was observed only in $Grn^{-/-}$ but not in $Grn^{+/-}$ mice, consistent with previous reports that lipofuscinosis and transcriptional changes are detected only in the complete absence of PGRN [38, 40, 44]. Interestingly, in contrast to prion-infected mice, PGRN haploinsufficiency has been shown to influence Aβ load and deposition in AD mouse models [52]. The time-dependent effects of PGRN deficiency on microglial function may explain conflicting observations across AD models. In some studies, $Grn^{-/-}$ mice exhibit increased amyloid deposits due to overactivated microglia with defective phagocytic capacity [50, 51], while others report reduced plaque burden due to more efficient phagocytosis and clearance by microglia at early stages [49, 52, 84].

While our data demonstrate enhanced microglial PrP^{Sc} clearance in $Grn^{-/-}$ mice at 120 dpi, we considered alternative explanations for reduced deposition, including impaired PrP^{Sc} propagation due to altered neuronal membrane dynamics or autophagic-lysosomal dysfunction. The temporal glial response progresses through distinct phases: early microglial activation and hyperphagocytosis coincides with moderate astrocyte activation, synergistically enhancing prion clearance. This protective phase was followed by late microglial overactivation and impaired prion clearance that drives increased astrogliosis. The eventual convergence of astrocyte marker and PrP^{Sc} deposition at the terminal stage likely reflects the different incubation periods of $Grn^{-/-}$ and $Grn^{+/+}$ mice. Collectively, these temporal shifts suggest that PGRN ablation initially boosts clearance capacity but ultimately drives maladaptive gliosis, consistent with our RNA-seq showing microglial polarization toward inflammatory states at 150 dpi.

To investigate how PGRN depletion enhances microglial activation during prion infection, we generated microglia-specific *Grn* knockout mice by crossing

CX3CR1-CreERT2 with $Grn^{fl/fl}$ mice. Intriguingly, in contrast to systemic PGRN deficiency, microglia-restricted depletion of PGRN did not alter prion pathogenesis. Thus, the heightened microglial activation seen in prion-infected $Grn^{-/-}$ mice likely involves non-cell-autonomous mechanisms and the complete PGRN ablation may be necessary to impact prion pathogenesis. This aligns with previous findings that neuronal-specific *Grn* knockout mice do not develop any neuropathological phenotypes observed in complete *Grn* knockout mice, and microglia-specific PGRN depletion does not exacerbate behavioral or pathological phenotypes in neuronal PGRN-insufficient mice [85, 86]. Further studies are needed to explore how different PGRN-expressing cell types interact in the brain and whether PGRN released from these cells influence prion pathogenesis.

While impaired autophagy and TDP-43 accumulation have been reported in aged $Grn^{-/-}$ mice [39], we observed no significant differences in autophagy-related proteins between prion-infected $Grn^{-/-}$ and control mice. This suggests that prion and TDP-43 employ distinct mechanisms for intracellular clearance and that accelerated prion progression in $Grn^{-/-}$ mice is not due to exacerbated autophagic impairment.

Dysfunctional lysosome, increased complement production, and enhanced synaptic pruning have been observed in aged $Grn^{-/-}$ mice [40]. Additionally, $Grn^{-/-}$ microglia promote TDP-43 granule formation, nuclear pore defects, and excitatory neuronal death via complement activation [42]. These phenotypes can be mitigated by depleting complement genes or blocking the complement cascade, indicating that PGRN suppresses excessive complement activation. In prion-infected $Grn^{-/-}$ mice, we observed aggravated complement activation at 150dpi, which may contribute to accelerated disease progression. Further studies are warranted to determine whether blocking of complement cascade (such as intercrossing $C1qa^{-/-}$ or $C3^{-/-}$ mice to $Grn^{-/-}$ mice) could mitigate the effects of PGRN depletion on prion disease.

We previously reported that TREM2 deficiency attenuates microglial activation in prion infected mice [56]. Together with the present findings, these results suggest that TREM2 and PGRN have opposing effects on prion-induced microglial activation. Indeed, loss of TREM2 and PGRN result in opposite microglial activation states [87]. While TREM2 ablation or antagonism can rescue the microglial hyperactivation in $Grn^{-/-}$ mice, it does not alleviate lysosomal dysfunction or neurotoxicity [88]. Furthermore, the transition of microglia from a homeostatic state to a disease-associated phenotype stage 2 depends on TREM2 signaling [69]. Thus, it would be interesting to investigate whether TREM2 depletion could dampen microglial hyperactivation and rescue the accelerated prion progression in $Grn^{-/-}$ mice.

Several strategies to increase PGRN levels have shown promise in treating FTD-GRN patients [1]. These include blocking PGRN degradation using anti-sortilin antibodies, supplementing recombinant PGRN via protein transport vehicle (PTV)-PGRN biologics, gene therapy employing adeno-associated virus (AAV)-mediated PGRN expression and small molecules to enhance expression of PGRN. However, further research is needed to determine whether these approaches could also benefit prion diseases.

Limitations of the study

While our study demonstrates a neuroprotective role for PGRN in a mouse model of prion infection, further research is needed to elucidate the role of PGRN in prion-induced neurodegeneration. Prion diseases are highly heterogenous, with different strains exhibiting unique characteristics, including variations in clinical symptoms, incubation periods, disease progression rates and brain regional lesion profiles [89]. In mouse models of scrapie prions, the widely studied RML, ME7 and 22 L strains display differences in cellular tropism of PrP^{Sc} accumulation and neuropathological distribution [90]. RML strain was selected for this study due to its thalamic preference, a brain region particularly vulnerable to PGRN deficiency [40]. While our findings demonstrate that ablation of PGRN alters prion pathology in RML-infected mice, the extent to which PGRN deficiency influences pathogenesis induced by other prion strains warrants further investigation. Notably, it remains unclear whether loss-of-function *GRN* variants are associated with an increased risk of prion diseases in humans, partly due to the rarity of conditions like Creutzfeldt-Jakob disease (CJD), Gerstmann-Sträussler-Scheinker syndrome (GSS), and fatal familial insomnia (FFI). Therefore, the relevance of *GRN* variants and PGRN dysfunction in human prion diseases warrants further investigation.

Conclusions

In summary, our study reveals a neuroprotective role for PGRN in prion disease. Microglia respond to prion infection in a stepwise manner, and PGRN restricts prion-induced microglial activation and decelerates prion pathology partly by suppressing excessive complement cascade activation. Given that PGRN overexpression or exogenous delivery has shown therapeutic benefits in other neurogenerative diseases [45, 50, 91–93], we propose that elevating PGRN levels - whether through small molecules, anti-sortilin antibodies, supplementation (e.g., PTV: PGRN biologics), or boosting expression (e.g., AAV-mediated gene therapy) - could represent a potential therapeutic strategy for prion disease.

Abbreviations

AAV	Adeno-associated virus
AD	Alzheimer's disease
ALS	Amyotrophic lateral sclerosis
CBS	Corticobasal syndrome
CJD	Creutzfeldt-Jacob disease
CNS	Central nervous system
dpi	Days post-inoculation
FFI	Fatal familial insomnia
FTLD	Frontotemporal lobar degeneration
GRN/Grn	Gene encoding progranulin in human or mouse
GSS	Gerstmann-Straussler-Scheinker syndrome
GWAS	Genome-wide association studies
LATE	Limbic-predominant age-related TDP-43 encephalopathy
NCL	Neuronal ceroid lipofuscinosis
PD	Parkinson's disease
PGRN	Progranulin
PrP	Prion protein
PTV	Protein transport vehicle
qRT-PCR	Quantitative reverse transcription polymerase chain reaction
RML6	Rocky Mountain Laboratory strain of mouse-adapted scrapie prions, passage 6
TDP-43	Transactivation response DNA binding protein-43
TREM2	Triggering receptor expressed on myeloid cells 2

Supplementary Information

The online version contains supplementary material available at https://doi.org/10.1186/s40478-025-02128-3.

Supplementary Material 1: **Supplementary Figure 1**. Full images of the cropped Western blots in figures. (a) Fig. 1b. (b) Fig. 4c. (c) Fig. 4f. (d-e) Fig. 6b. (f-g) Fig. 6d. (h-i) Fig. 6f. (a') shows the validation of PGRN antibody specificity by ***Grn*** KO BV2 cells generated by CRISPR-Cas9.

Supplementary Material 2: **Supplementary Figure 2**. Ribosomal profiling of ***Grn*** expression in CamKIIa^{+} cortical (a) and hippocampal neurons (b), PV neurons (c) and astrocytes (d) at different time points after prion inoculation (n = 3, except n = 2 for cortical neurons at terminal stage and GFAP^{+} astrocytes at 2 wpi). ns: $P > 0.05$; **: $P < 0.01$.

Supplementary Material 3: **Supplementary Figure 3**. Representative histology of various brain regions from NBH-inoculated ***Grn***$^{-/-}$ and ***Grn***$^{+/+}$ (WT) mice stained for H&E (a), SAF84 (b), GFAP (c) and Iba-1 (d). Scale bar: 100μm in (a) and (b), 25μm in (c) and (d).

Supplementary Material 4: **Supplementary Figure 4**. (a) Plot of microglial numbers at 120 dpi, 150 dpi and terminal stage. (b) Plot of SAF84 signals at 120 dpi, 150 dpi and terminal stage. (c) Left: Total PrP Western blot of homogenates prepared from RML6-infected ***Grn***$^{-/-}$, ***Grn***$^{+/-}$ and ***Grn***$^{+/+}$ (WT) mouse brains at 120 dpi. Right, densitometric quantification of the total PrP Western blot. n = 3. (d) Representative histology of H&E staining of thalamus from RML6-infected ***Grn***$^{-/-}$, ***Grn***$^{+/-}$ and ***Grn***$^{+/+}$ (WT) littermates at 120 dpi. Scale bars: 100μm. (e) Left, representative histology of GFAP immunohistochemistry of thalamus from RML6-infected ***Grn***$^{-/-}$, ***Grn***$^{+/-}$ and ***Grn***$^{+/+}$ (WT) littermates at 120 dpi. Scale bar:25μm. Right: quantification of GFAP^{+} cells at thalamus. n = 6 ~ 16. ns: $P > 0.05$.

Supplementary Material 5: **Supplementary Figure 5**. (a) Multidimensional scaling (MDS) plot of RNAseq data for microglia (CD11b^{+}) from prion-infected ***Grn***$^{-/-}$, ***Grn***$^{+/-}$ and ***Grn***$^{+/+}$ (WT) mouse brains at 150 dpi. n = 3 for ***Grn***$^{-/-}$ mice, n = 4 for ***Grn***$^{+/-}$ mice, n = 3 for ***Grn***$^{+/+}$ (WT) mice. (b) Venn diagram of overlapping DEGs between microglia from prion infected ***Grn***$^{-/-}$ v.s ***Grn***$^{+/+}$ mice and ***Grn***$^{-/-}$ v.s ***Grn***$^{+/+}$ mice at 7 months old. (c) Venn diagram of overlapping DEGs between microglia from prion infected ***Grn***$^{-/-}$ v.s ***Grn***$^{+/+}$ mice and ***Grn***$^{-/-}$ v.s ***Grn***$^{+/+}$ mice at 7-, 12- and 19- months old. (d) RNA-Seq data of ***Cd22*** expression in hippocampi at different time points after prion inoculation (n = 3). (e) RNA-Seq data of ***Cd22*** expression in sorted microglia (CD11b^{+}) at different time points after prion inoculation (n = 5). (f) qRT-PCR of ***Cd22*** expression in noninfected ***Grn***$^{-/-}$ v.s ***Grn***$^{+/+}$ mouse brains (n = 5 ~ 6). (g) qRT-PCR of ***Cd22*** expression in noninfected ***Grn***$^{-/-}$ v.s ***Grn***$^{+/+}$ BV2 microglia (n = 3). ***: $P < 0.001$; ****: $P < 0.0001$.

Supplementary Material 6: **Supplementary Figure 6**. (a-b) RNA-Seq data of ***C1qa*** (a) ***and C3*** (b) expression in hippocampi at different time points after prion inoculation (n = 3). (c-d) RNA-Seq data of ***C1qa*** (c) ***and C3*** (d) expression in sorted microglia (CD11b^{+}) at different time points after prion inoculation (n = 5). (e) Left, Western blot of LC3B in prion-infected ***Grn***$^{-/-}$, ***Grn***$^{+/-}$ and ***Grn***$^{+/+}$ (WT) mouse brains at 150 dpi. Right, densitometric quantification of the LC3B Western blot. n = 3 for ***Grn***$^{+/-}$ and ***Grn***$^{+/+}$ (WT) mice, n = 4 for ***Grn***$^{-/-}$ mice. (f) Left, Western blot of P62 in prion-infected ***Grn***$^{-/-}$ mice at 150 dpi. Right, densitometric quantification of the P62 Western blot. n = 3 for ***Grn***$^{+/-}$ and ***Grn***$^{+/+}$ (WT) mice, n = 4 for ***Grn***$^{-/-}$ mice. ns: $P > 0.05$; *: $P < 0.05$; **: $P < 0.01$; ****: $P < 0.0001$.

Supplementary Material 7: **Supplementary Figure 7**. (a-c) qRT-PCR of ***C1qa***, ***C3*** and ***Cd22*** mRNA in RML6-infected CX3CR1-CreERT; ***Grn***$^{fl/fl}$ and ***Grn***$^{fl/fl}$ brains at terminal stage. n = 5 ~ 6. (d) Immunofluorescence staining of PGRN and Iba-1 on brain sections from RML6- and NBH-inoculated mice, arrows indicate the PGRN signals in Iba-1^{+} microglia. Scale bar: 20μm. ns: $P > 0.05$.

Supplementary Material 8: **Supplementary Table 1**. RNA-seq data of microglia (CD11b^{+}) isolated from RML6-infected ***Grn***$^{-/-}$, ***Grn***$^{+/-}$ and ***Grn***$^{+/+}$ (WT) mouse brains at 150 dpi. The overlapping differentially expressed genes (DEGs) with snRNA-seq data of Zhang et al study in Supplementary Figure. 5b-c were highlighted.

Acknowledgements

We thank the teams of the Institute of Neuropathology, University Hospital Zurich and Department of Neurobiology, School of Basic Medical Sciences of Fudan University for technical assistance. We also thank Masugi Nishihara from University of Tokyo for providing us with Grn / mice, and thank Robert V Farese Jr from Harvard T. H. Chan School of Public Health for sharing us Grnflox/flox mice. We thank Prof. Elisabeth J. Rushing for reading and editing the article.

Author contributions

C.Z. and A.A. planned and conceived study. B.L., Y.S., W.H., H.G., J.L., T.Y., W.L., D.C. and C.Z. performed and analyzed the biochemical and histological experiments. P.S. performed prion inoculation experiments. RNA-seq was performed in Functional Genomic Center Zurich (FGCZ). C.Z. and A.A. supervised the execution of the project. B.L., C.Z. and A.A. wrote the manuscript with input and revisions from all authors.

Funding

C. Zhu is sponsored by Research Startup Funds of Fudan University, National Natural Science Foundation of China (No. 82271476 and No. 82071436), Shanghai Pujiang Program (No. 20PJ1401100), and The Program for Oriental Scholars of Shanghai Universities (Distinguished Professor) (No. TP2022050). B. Li is supported by National Natural Science Foundation of China (No. 82101502) and China Postdoctoral Science Foundation (No. 2021M690036). A. Aguzzi is the recipient of an Advanced Grant of the European Research Council (ERC, No. 670958) and is supported by grants from the European Union (PRIORITY, NEURINOX), the Swiss National Foundation (SNF, including a Sinergia grant), the Swiss Initiative in Systems Biology, SystemsX.ch (PrionX, SynucleiX), and a Distinguished Scientist Award of the Nomis Foundation. The funders had no role in study design, data collection and analysis, decision to publish, or preparation of the manuscript.

Data availability

Additional information is available upon reasonable request.

Declarations

Ethics approval and consent to participate

All animal experiments were carried out in strict accordance with the Rules and Regulations for the Protection of Animal Rights (Tierschutzgesetz and Tierschutzverordnung) of the Swiss Bundesamt für Lebensmittelsicherheit und Veterinärwesen and were preemptively approved by the Animal Welfare Committee of the Canton of Zürich (permit ZH040/2015).

Consent for publication

Not applicable.

Competing interests
The authors declare no competing interests.

Received: 23 May 2025 / Accepted: 15 September 2025
Published online: 13 October 2025

References

1. Rhinn H, Tatton N, McCaughey S, Kurnellas M, Rosenthal A (2022) Progranulin as a therapeutic target in neurodegenerative diseases. Trends Pharmacol Sci: https://doi.org/10.1016/j.tips.2021.11.015
2. Van Damme P, Van Hoecke A, Lambrechts D, Vanacker P, Bogaert E, Van Swieten J, Carmeliet P, Van den Bosch L, Robberecht W (2008) Progranulin functions as a neurotrophic factor to regulate neurite outgrowth and enhance neuronal survival. J Cell Biol 181:37–41. https://doi.org/10.1083/jcb.200712039
3. Xu J, Xilouri M, Bruban J, Shioi J, Shao Z, Papazoglou I, Vekrellis K, Robakis NK (2011) Extracellular progranulin protects cortical neurons from toxic insults by activating survival signaling. Neurobiol Aging 32(2326 e2325–2316). https://doi.org/10.1016/j.neurobiolaging.2011.06.017
4. Baker M, Mackenzie IR, Pickering-Brown SM, Gass J, Rademakers R, Lindholm C, Snowden J, Adamson J, Sadovnick AD, Rollinson Set al et al (2006) Mutations in progranulin cause tau-negative frontotemporal dementia linked to chromosome 17. Nature 442:916–919. https://doi.org/10.1038/nature05016
5. Cruts M, Gijselinck I, van der Zee J, Engelborghs S, Wils H, Pirici D, Rademakers R, Vandenberghe R, Dermaut B Martin JJ (2006) null mutations in progranulin cause ubiquitin-positive frontotemporal dementia linked to chromosome 17q21. Nature 442:920–924 https://doi.org/10.1038/nature05017
6. Gass J, Cannon A, Mackenzie IR, Boeve B, Baker M, Adamson J, Crook R, Melquist S, Kuntz K, Petersen Ret al et al (2006) Mutations in progranulin are a major cause of ubiquitin-positive frontotemporal Lobar degeneration. Hum Mol Genet 15:2988–3001. https://doi.org/10.1093/hmg/ddl241
7. Leverenz JB, Yu CE, Montine TJ, Steinbart E, Bekris LM, Zabetian C, Kwong LK, Lee VM, Schellenberg GD, Bird TD (2007) A novel progranulin mutation associated with variable clinical presentation and tau, TDP43 and alpha-synuclein pathology. Brain 130:1360–1374. https://doi.org/10.1093/brain/awm069
8. Neumann M, Sampathu DM, Kwong LK, Truax AC, Micsenyi MC, Chou TT, Bruce J, Schuck T, Grossman M, Clark CMet al et al (2006) Ubiquitinated TDP-43 in frontotemporal Lobar degeneration and amyotrophic lateral sclerosis. Science 314:130–133. https://doi.org/10.1126/science.1134108
9. Hu F, Padukkavidana T, Vaegter CB, Brady OA, Zheng Y, Mackenzie IR, Feldman HH, Nykjaer A, Strittmatter SM (2010) Sortilin-mediated endocytosis determines levels of the frontotemporal dementia protein, progranulin. Neuron 68:654–667. https://doi.org/10.1016/j.neuron.2010.09.034
10. Zhou X, Sun L, Bastos de Oliveira F, Qi X, Brown WJ, Smolka MB, Sun Y, Hu F (2015) Prosaposin facilitates sortilin-independent lysosomal trafficking of progranulin. J Cell Biol 210:991–1002. https://doi.org/10.1083/jcb.201502029
11. Almeida S, Gao F, Coppola G, Gao FB (2016) Suberoylanilide hydroxamic acid increases progranulin production in iPSC-derived cortical neurons of frontotemporal dementia patients. Neurobiol Aging 42:35–40. https://doi.org/10.1016/j.neurobiolaging.2016.03.001
12. Canafoglia L, Morbin M, Scaioli V, Pareyson D, D'Incerti L, Fugnanesi V, Tagliavini F, Berkovic SF, Franceschetti S (2014) Recurrent generalized seizures, visual loss, and palinopsia as phenotypic features of neuronal ceroid lipofuscinosis due to progranulin gene mutation. Epilepsia 55:e56–e59. https://doi.org/10.1111/epi.12632
13. Faber I, Prota JR, Martinez AR, Lopes-Cendes I, Franca MCJ (2017) A new phenotype associated with homozygous GRN mutations: complicated spastic paraplegia. Eur J Neurol 24:e3–e4. https://doi.org/10.1111/ene.13194
14. Huin V, Barbier M, Bottani A, Lobrinus JA, Clot F, Lamari F, Chat L, Rucheton B, Fluchere F, Auvin Set al et al (2020) Homozygous GRN mutations: new phenotypes and new insights into pathological and molecular mechanisms. Brain 143:303–319. https://doi.org/10.1093/brain/awz377
15. Kamate M, Detroja M, Hattiholi V (2019) Neuronal ceroid lipofuscinosis type-11 in an adolescent. Brain Dev 41:542–545. https://doi.org/10.1016/j.braindev.2019.03.004
16. Smith KR, Damiano J, Franceschetti S, Carpenter S, Canafoglia L, Morbin M, Rossi G, Pareyson D, Mole SE, Staropoli JFet al et al (2012) Strikingly different clinicopathological phenotypes determined by progranulin-mutation dosage. Am J Hum Genet 90:1102–1107. https://doi.org/10.1016/j.ajhg.2012.04.021
17. Brouwers N, Sleegers K, Engelborghs S, Maurer-Stroh S, Gijselinck I, van der Zee J, Pickut BA, Van den Broeck M, Mattheijssens M, Peeters K al (2008) Genetic variability in progranulin contributes to risk for clinically diagnosed alzheimer disease. Neurology 71:656–664. https://doi.org/10.1212/01.wnl.0000319688.89790.7a
18. Cruchaga C, Haller G, Chakraverty S, Mayo K, Vallania FL, Mitra RD, Faber K, Williamson J, Bird T, Diaz-Arrastia R et al (2012) Rare variants in APP, PSEN1 and PSEN2 increase risk for AD in late-onset Alzheimer's disease families. PLoS One 7:e31039 https://doi.org/10.1371/journal.pone.0031039
19. Fenoglio C, Galimberti D, Cortini F, Kauwe JS, Cruchaga C, Venturelli E, Villa C, Serpente M, Scalabrini D, Mayo K et al (2009) Rs5848 variant influences GRN mRNA levels in brain and peripheral mononuclear cells in patients with Alzheimer's disease. J Alzheimers Dis 18:603–612 https://doi.org/10.3233/JAD-2009-1170
20. Hsiung GY, Fok A, Feldman HH, Rademakers R, Mackenzie IR (2011) rs5848 polymorphism and serum progranulin level. J Neurol Sci 300:28–32. https://doi.org/10.1016/j.jns.2010.10.009
21. Lee MJ, Chen TF, Cheng TW, Chiu MJ (2011) rs5848 variant of progranulin gene is a risk of alzheimer's disease in the Taiwanese population. Neurodegener Dis 8:216–220. https://doi.org/10.1159/000322538
22. Perry DC, Lehmann M, Yokoyama JS, Karydas A, Lee JJ, Coppola G, Grinberg LT, Geschwind D, Seeley WW, Miller BLet al et al (2013) Progranulin mutations as risk factors for alzheimer disease. Jama Neurol 70:774–778. https://doi.org/10.1001/2013.jamaneurol.393
23. Sheng JH, Su LL, Xu ZP, Chen GD (2014) Progranulin polymorphism rs5848 is associated with increased risk of alzheimer's disease. Gene 542:141–145. https://doi.org/10.1016/j.gene.2014.03.041
24. Vardarajan BN, Reyes-Dumeyer D, Piriz AL, Lantigua RA, Medrano M, Rivera D, Jimenez-Velazquez IZ, Martin E, Pericak-Vance MA, Bush W et al (2022) Progranulin mutations in clinical and neuropathological Alzheimer's disease. Alzheimers Dement: https://doi.org/10.1002/alz.12567
25. Viswanathan J, Makinen P, Helisalmni S, Haapasalo A, Soininen H, Hiltunen M (2009) An association study between granulin gene polymorphisms and alzheimer's disease in Finnish population. Am J Med Genet B 150b:747–750. https://doi.org/10.1002/ajmg.b.30889
26. Xu HM, Tan L, Wan Y, Tan MS, Zhang W, Zheng ZJ, Kong LL, Wang ZX, Jiang T, Tan L al (2017) PGRN is associated with Late-Onset alzheimer's disease: a Case-Control replication study and Meta-analysis. Mol Neurobiol 54:1187–1195. https://doi.org/10.1007/s12035-016-9698-4
27. Nalls MA, Blauwendraat C, Vallerga CL, Heilbron K, Bandres-Ciga S, Chang D, Tan M, Kia DA, Noyce AJ, Xue A al (2019) Identification of novel risk loci, causal insights, and heritable risk for parkinson's disease: a meta-analysis of genome-wide association studies. Lancet Neurol 18:1091–1102. https://doi.org/10.1016/S1474-4422(19)30320-5
28. Sleegers K, Brouwers N, Maurer-Stroh S, van Es MA, Van Damme P, van Vught PW, van der Zee J, Serneels S, De Pooter T Broeck M et al (2008) Progranulin genetic variability contributes to amyotrophic lateral sclerosis. Neurology 71:253–259 https://doi.org/10.1212/01.wnl.0000289191.54852.75
29. Masellis M, Momeni P, Meschino W, Heffner R Jr., Elder J, Sato C, Liang Y, St George-Hyslop P, Hardy J, Bilbao Jet al et al (2006) Novel splicing mutation in the progranulin gene causing Familial corticobasal syndrome. Brain 129:3115–3123. https://doi.org/10.1093/brain/awl276
30. Redaelli V, Rossi G, Maderna E, Kovacs GG, Piccoli E, Caroppo P, Cacciatore F, Spinello S, Grisoli M, Sozzi G al (2018) Alzheimer neuropathology without frontotemporal Lobar degeneration hallmarks (TAR DNA-binding protein 43 inclusions) in missense progranulin mutation Cys139Arg. Brain Pathol 28:72–76. https://doi.org/10.1111/bpa.12480
31. Nelson PT, Dickson DW, Trojanowski JQ, Jack CR, Boyle PA, Arfanakis K, Rademakers R, Alafuzoff I, Attems J, Brayne Cet al et al (2019) Limbic-predominant age-related TDP-43 encephalopathy (LATE): consensus working group report. Brain 142:1503–1527. https://doi.org/10.1093/brain/awz099
32. Reho P, Koga S, Shah Z, Chia R, International LBDGC, American Genome C, Rademakers R, Dalgard CL, Boeve BF, Beach TG et al (2022) GRN Mutations Are Associated with Lewy Body Dementia. Mov Disord: https://doi.org/10.1002/mds.29144
33. Kayasuga Y, Chiba S, Suzuki M, Kikusui T, Matsuwaki T, Yamanouchi K, Kotaki H, Horai R, Iwakura Y, Nishihara M (2007) Alteration of behavioural phenotype in mice by targeted disruption of the progranulin gene. Behav Brain Res 185:110–118. https://doi.org/10.1016/j.bbr.2007.07.020
34. Martens LH, Zhang J, Barmada SJ, Zhou P, Kamiya S, Sun B, Min SW, Gan L, Finkbeiner S, Huang EJ al (2012) Progranulin deficiency promotes

neuroinflammation and neuron loss following toxin-induced injury. J Clin Invest 122:3955–3959. https://doi.org/10.1172/JCI63113
35. Petkau TL, Neal SJ, Milnerwood A, Mew A, Hill AM, Orban P, Gregg J, Lu G, Feldman HH, Mackenzie IR et al (2012) Synaptic dysfunction in progranulin-deficient mice. Neurobiol Dis 45:711–722 https://doi.org/10.1016/j.nbd.2011.10.016
36. Wils H, Kleinberger G, Pereson S, Janssens J, Capell A, Van Dam D, Cuijt I, Joris G, De Deyn PP, Haass Cet al et al (2012) Cellular ageing, increased mortality and FTLD-TDP-associated neuropathology in progranulin knockout mice. J Pathol 228:67–76. https://doi.org/10.1002/path.4043
37. Yin F, Banerjee R, Thomas B, Zhou P, Qian L, Jia T, Ma X, Ma Y, Iadecola C Beal MF (2010) exaggerated inflammation, impaired host defense, and neuropathology in progranulin-deficient mice. J Exp Med 207:117–128 https://doi.org/10.1084/jem.20091568
38. Ahmed Z, Sheng H, Xu YF, Lin WL, Innes AE, Gass J, Yu X, Wuertzer CA, Hou H, Chiba Set al et al (2010) Accelerated lipofuscinosis and ubiquitination in granulin knockout mice suggest a role for progranulin in successful aging. Am J Pathol 177:311–324. https://doi.org/10.2353/ajpath.2010.090915
39. Chang MC, Srinivasan K, Friedman BA, Suto E, Modrusan Z, Lee WP, Kaminker JS, Hansen DV, Sheng M (2017) Progranulin deficiency causes impairment of autophagy and TDP-43 accumulation. J Exp Med 214:2611–2628. https://doi.org/10.1084/jem.20160999
40. Lui H, Zhang J, Makinson SR, Cahill MK, Kelley KW, Huang HY, Shang Y, Oldham MC, Martens LH, Gao Fet al et al (2016) Progranulin deficiency promotes Circuit-Specific synaptic pruning by microglia via complement activation. Cell 165:921–935. https://doi.org/10.1016/j.cell.2016.04.001
41. Wu Y, Shao W, Todd TW, Tong J, Yue M, Koga S, Castanedes-Casey M, Librero AL, Lee CW, Mackenzie IR al (2021) Microglial lysosome dysfunction contributes to white matter pathology and TDP-43 proteinopathy in GRN-associated FTD. Cell Rep 36:109581. https://doi.org/10.1016/j.celrep.2021.109581
42. Zhang J, Velmeshev D, Hashimoto K, Huang YH, Hofmann JW, Shi X, Chen J, Leidal AM, Dishart JG Cahill MK (2020) neurotoxic microglia promote TDP-43 proteinopathy in progranulin deficiency. Nature 588:459–465 https://doi.org/10.1038/s41586-020-2709-7
43. Boland S, Swarup S, Ambaw YA, Malia PC, Richards RC, Fischer AW, Singh S, Aggarwal G, Spina S, Nana ALet al et al (2022) Deficiency of the frontotemporal dementia gene GRN results in gangliosidosis. Nat Commun 13:5924. https://doi.org/10.1038/s41467-022-33500-9
44. Evers BM, Rodriguez-Navas C, Tesla RJ, Prange-Kiel J, Wasser CR, Yoo KS, McDonald J, Cenik B, Plattner Ravenscroft TA F et al (2017) Lipidomic and Transcriptomic Basis of Lysosomal Dysfunction in Progranulin Deficiency. Cell Rep 20:2565–2574 https://doi.org/10.1016/j.celrep.2017.08.056
45. Logan T, Simon MJ, Rana A, Cherf GM, Srivastava A, Davis SS, Low RLY, Chiu CL, Fang M, Huang F (2021) al Rescue of a lysosomal storage disorder caused by Grn loss of function with a brain penetrant progranulin biologic. Cell 184:4651–4668 e4625 https://doi.org/10.1016/j.cell.2021.08.002
46. Marschallinger J, Iram T, Zardeneta M, Lee SE, Lehallier B, Haney MS, Pluvinage JV, Mathur V, Hahn O, Morgens DW al (2020) Lipid-droplet-accumulating microglia represent a dysfunctional and Proinflammatory state in the aging brain. Nat Neurosci 23:194–208. https://doi.org/10.1038/s41593-019-0566-1
47. Gerrits E, Giannini LAA, Brouwer N, Melhem S, Seilhean D, Le Ber I, Brainbank Neuro CEBNN, Kamermans A, Kooij G, de Vries HE et al (2022) Neurovascular dysfunction in GRN-associated frontotemporal dementia identified by single-nucleus RNA sequencing of human cerebral cortex. Nat Neurosci 25:1034–1048 https://doi.org/10.1038/s41593-022-01124-3
48. Hosokawa M, Arai T, Masuda-Suzukake M, Kondo H, Matsuwaki T, Nishihara M, Hasegawa M, Akiyama H (2015) Progranulin reduction is associated with increased Tau phosphorylation in P301L Tau Transgenic mice. J Neuropath Exp Neur 74:158–165. https://doi.org/10.1097/Nen.0000000000000158
49. Takahashi H, Klein ZA, Bhagat SM, Kaufman AC, Kostylev MA, Ikezu T, Strittmatter SM, Alzheimer's Disease Neuroimaging I (2017) Opposing effects of progranulin deficiency on amyloid and Tau pathologies via microglial TYROBP network. Acta Neuropathol 133:785–807. https://doi.org/10.1007/s00401-017-1668-z
50. Minami SS, Min SW, Krabbe G, Wang C, Zhou Y, Asgarov R, Li Y, Martens LH, Elia LP, Ward MEet al et al (2014) Progranulin protects against amyloid beta deposition and toxicity in alzheimer's disease mouse models. Nat Med 20:1157–1164. https://doi.org/10.1038/nm.3672
51. Van Kampen JM, Kay DG (2017) Progranulin gene delivery reduces plaque burden and synaptic atrophy in a mouse model of alzheimer's disease. PLoS ONE 12:e0182896. https://doi.org/10.1371/journal.pone.0182896
52. Hosokawa M, Tanaka Y, Arai T, Kondo H, Akiyama H, Hasegawa M (2018) Progranulin haploinsufficiency reduces amyloid beta deposition in alzheimer's disease model mice. Exp Anim 67:63–70. https://doi.org/10.1538/expanim.17-0060
53. Aguzzi A, Nuvolone M, Zhu C (2013) The immunobiology of prion diseases. Nat Rev Immunol 13:888–902. https://doi.org/10.1038/nri3553
54. Aguzzi A, Zhu C (2017) Microglia in prion diseases. J Clin Invest 127:3230–3239. https://doi.org/10.1172/JCI90605
55. Zhu C, Herrmann US, Falsig J, Abakumova I, Nuvolone M, Schwarz P, Frauenknecht K, Rushing EJ, Aguzzi A (2016) A neuroprotective role for microglia in prion diseases. J Exp Med 213:1047–1059. https://doi.org/10.1084/jem.20151000
56. Zhu C, Herrmann US, Li B, Abakumova I, Moos R, Schwarz P, Rushing EJ, Colonna M, Aguzzi A (2015) Triggering receptor expressed on myeloid cells-2 is involved in prion-induced microglial activation but does not contribute to prion pathogenesis in mouse brains. Neurobiol Aging 36:1994–2003. https://doi.org/10.1016/j.neurobiolaging.2015.02.019
57. Lopez-Perez O, Badiola JJ, Bolea R, Ferrer I, Llorens F, Martin-Burriel I (2020) An update on autophagy in prion diseases. Front Bioeng Biotechnol 8:975. https://doi.org/10.3389/fbioe.2020.00975
58. Majumder P, Chakrabarti O (2018) Lysosomal quality control in prion diseases. Mol Neurobiol 55:2631–2644. https://doi.org/10.1007/s12035-017-0512-8
59. Parkhurst CN, Yang G, Ninan I, Savas JN, Yates JR 3rd, Lafaille JJ, Hempstead BL, Littman DR, Gan WB (2013) Microglia promote learning-dependent synapse formation through brain-derived neurotrophic factor. Cell 155:1596–1609. https://doi.org/10.1016/j.cell.2013.11.030
60. Bueler H, Fischer M, Lang Y, Bluethmann H, Lipp HP, DeArmond SJ, Prusiner SB, Aguet M, Weissmann C (1992) Normal development and behaviour of mice lacking the neuronal cell-surface PrP protein. Nature 356:577–582. https://doi.org/10.1038/356577a0
61. Zhu C, Schwarz P, Abakumova I, Aguzzi A (2015) Unaltered prion pathogenesis in a mouse model of High-Fat Diet-Induced insulin resistance. PLoS ONE 10:e0144983. https://doi.org/10.1371/journal.pone.0144983
62. Li B, Dewey CN (2011) RSEM: accurate transcript quantification from RNA-Seq data with or without a reference genome. Bmc Bioinf 12: Doi Artn 323. https://doi.org/10.1186/1471-2105-12-323
63. Love MI, Huber W, Anders S (2014) Moderated Estimation of fold change and dispersion for RNA-seq data with DESeq2. Genome Biol 15:550. https://doi.org/10.1186/s13059-014-0550-8
64. Sorce S, Nuvolone M, Russo G, Chincisan A, Heinzer D, Avar M, Pfammatter M, Schwarz P, Delic M, Muller M al (2020) Genome-wide transcriptomics identifies an early preclinical signature of prion infection. PLoS Pathog 16:e1008653. https://doi.org/10.1371/journal.ppat.1008653
65. Scheckel C, Imeri M, Schwarz P, Aguzzi A (2020) Ribosomal profiling during prion disease uncovers progressive translational derangement in glia but not in neurons. Elife 9. https://doi.org/10.7554/eLife.62911
66. Bartoletti-Stella A, Corrado P, Mometto N, Baiardi S, Durrenberger PF, Arzberger T, Reynolds R, Kretzschmar H, Capellari S, Parchi P (2019) Analysis of RNA expression profiles identifies dysregulated vesicle trafficking pathways in Creutzfeldt-Jakob disease. Mol Neurobiol 56:5009–5024. https://doi.org/10.1007/s12035-018-1421-1
67. Marsan E, Velmeshev D, Ramsey A, Patel RK, Zhang J, Koontz M, Andrews MG, de Majo M, Mora C, Blumenfeld Jet al et al (2023) Astroglial toxicity promotes synaptic degeneration in the thalamocortical circuit in frontotemporal dementia with GRN mutations. J Clin Invest: https://doi.org/10.1172/JCI164919
68. Bordt EA, Block CL, Petrozziello T, Sadri-Vakili G, Smith CJ, Edlow AG, Bilbo SD (2020) Isolation of microglia from mouse or human tissue. STAR Protoc 1. https://doi.org/10.1016/j.xpro.2020.100035
69. Keren-Shaul H, Spinrad A, Weiner A, Matcovitch-Natan O, Dvir-Szternfeld R, Ulland TK, David E, Baruch K, Lara-Astaiso D, Toth B et al (2017) A Unique Microglia Type Associated with Restricting Development of Alzheimer's Disease. Cell 169:1276–1290 e1217 https://doi.org/10.1016/j.cell.2017.05.018
70. Aires V, Coulon-Bainier C, Pavlovic A, Ebeling M, Schmucki R, Schweitzer C, Kueng E, Gutbier S, Harde E (2021) CD22 blockage restores Age-Related impairments of microglia surveillance capacity. Front Immunol 12:684430. https://doi.org/10.3389/fimmu.2021.684430
71. Pluvinage JV, Haney MS, Smith BAH, Sun J, Iram T, Bonanno L, Li L, Lee DP, Morgens DW, Yang AC al (2019) CD22 Blockade restores homeostatic microglial phagocytosis in ageing brains. Nature 568:187–192. https://doi.org/10.1038/s41586-019-1088-4

72. Mabbott NA, Bruce ME, Botto M, Walport MJ, Pepys MB (2001) Temporary depletion of complement component C3 or genetic deficiency of C1q significantly delays onset of scrapie. Nat Med 7:485–487. https://doi.org/10.1038/86562
73. Coppola G, Karydas A, Rademakers R, Wang Q, Baker M, Hutton M, Miller BL, Geschwind DH (2008) Gene expression study on peripheral blood identifies progranulin mutations. Ann Neurol 64:92–96. https://doi.org/10.1002/ana.21397
74. Finch N, Baker M, Crook R, Swanson K, Kuntz K, Surtees R, Bisceglio G, Rovelet-Lecrux A, Boeve B Petersen RC (2009) plasma progranulin levels predict progranulin mutation status in frontotemporal dementia patients and asymptomatic family members. Brain 132:583–591 https://doi.org/10.1093/brain/awn352
75. Galimberti D, Fumagalli GG, Fenoglio C, Cioffi SMG, Arighi A, Serpente M, Borroni B, Padovani A, Tagliavini F, Masellis M (2018) al Progranulin plasma levels predict the presence of GRN mutations in asymptomatic subjects and do not correlate with brain atrophy: results from the GENFI study. Neurobiol Aging 62:245 e249-245 e212 https://doi.org/10.1016/j.neurobiolaging.2017.10.016
76. Ghidoni R, Benussi L, Glionna M, Franzoni M, Binetti G (2008) Low plasma progranulin levels predict progranulin mutations in frontotemporal Lobar degeneration. Neurology 71:1235–1239. https://doi.org/10.1212/01.wnl.0000325058.10218.fc
77. Ghidoni R, Stoppani E, Rossi G, Piccoli E, Albertini V, Paterlini A, Glionna M, Pegoiani E, Agnati LF Fenoglio C (2012) optimal plasma progranulin cutoff value for predicting null progranulin mutations in neurodegenerative diseases: a multicenter Italian study. Neurodegener Dis 9:121–127 https://doi.org/10.1159/000333132
78. Sleegers K, Brouwers N, Van Damme P, Engelborghs S, Gijselinck I, van der Zee J, Peeters K, Mattheijssens M, Cruts M, Vandenberghe R al (2009) Serum biomarker for progranulin-associated frontotemporal Lobar degeneration. Ann Neurol 65:603–609. https://doi.org/10.1002/ana.21621
79. Wilke C, Gillardon F, Deuschle C, Hobert MA, Jansen IE, Metzger FG, Heutink P, Gasser T, Maetzler W, Blauwendraat C et al (2017) Cerebrospinal Fluid Progranulin, but Not Serum Progranulin, Is Reduced in GRN-Negative Frontotemporal Dementia. Neurodegener Dis 17:83–88 https://doi.org/10.1159/000448896
80. Kamalainen A, Viswanathan J, Natunen T, Helisalmi S, Kauppinen T, Pikkarainen M, Pursiheimo JP, Alafuzoff I, Kivipelto M, Haapasalo A al (2013) GRN variant rs5848 reduces plasma and brain levels of granulin in alzheimer's disease patients. J Alzheimers Dis 33:23–27. https://doi.org/10.3233/JAD-2012-120946
81. Satoh J, Kino Y, Yamamoto Y, Kawana N, Ishida T, Saito Y, Arima K (2014) PLD3 is accumulated on neuritic plaques in Alzheimer's disease brains. Alzheimers Res Ther 6: Doi ARTN 70. https://doi.org/10.1186/s13195-014-0070-5
82. Suarez-Calvet M, Capell A, Caballero MAA, Morenas-Rodriguez E, Fellerer K, Franzmeier N, Kleinberger G, Eren E, Deming Y, Piccio L al (2018) CSF progranulin increases in the course of Alzheimer's disease and is associated with sTREM2, neurodegeneration and cognitive decline. Embo Mol Med 10 Doi ARTN e9712. https://doi.org/10.15252/emmm.2018097121
83. Pereson S, Wils H, Kleinberger G, McGowan E, Vandewoestyne M, Van Broeck B, Joris G, Cuijt I, Deforce D, Hutton M et al (2009) Progranulin expression correlates with dense-core amyloid plaque burden in Alzheimer disease mouse models. J Pathol 219:173–181 https://doi.org/10.1002/path.2580
84. Du H, Wong MY, Zhang T, Santos MN, Hsu C, Zhang J, Yu H, Luo W, Hu F (2021) A multifaceted role of progranulin in regulating amyloid-beta dynamics and responses. Life Sci Alliance 4. https://doi.org/10.26508/lsa.202000874
85. Arrant AE, Filiano AJ, Patel AR, Hoffmann MQ, Boyle NR, Kashyap SN, Onyilo VC, Young AH, Roberson ED (2019) Reduction of microglial progranulin does not exacerbate pathology or behavioral deficits in neuronal progranulin-insufficient mice. Neurobiol Dis 124:152–162. https://doi.org/10.1016/j.nbd.2018.11.011
86. Petkau TL, Blanco J, Leavitt BR (2017) Conditional loss of progranulin in neurons is not sufficient to cause neuronal ceroid lipofuscinosis-like neuropathology in mice. Neurobiol Dis 106:14–22. https://doi.org/10.1016/j.nbd.2017.06.012
87. Gotzl JK, Brendel M, Werner G, Parhizkar S, Sebastian Monasor L, Kleinberger G, Colombo AV, Deussing M, Wagner M, Winkelmann J al (2019) Opposite microglial activation stages upon loss of PGRN or TREM2 result in reduced cerebral glucose metabolism. Embo Mol Med 11. https://doi.org/10.15252/emmm.201809711
88. Reifschneider A, Robinson S, van Lengerich B, Gnorich J, Logan T, Heindl S, Vogt MA, Weidinger E, Riedl L, Wind Ket al et al (2022) Loss of TREM2 rescues hyperactivation of microglia, but not lysosomal deficits and neurotoxicity in models of progranulin deficiency. EMBO J 41:e109108. https://doi.org/10.15252/embj.2021109108
89. Carta M, Aguzzi A (2022) Molecular foundations of prion strain diversity. Curr Opin Neurobiol 72:22–31. https://doi.org/10.1016/j.conb.2021.07.010
90. Carroll JA, Striebel JF, Rangel A, Woods T, Phillips K, Peterson KE, Race B, Chesebro B (2016) Prion strain differences in accumulation of PrPSc on neurons and glia are associated with similar expression profiles of neuroinflammatory genes: comparison of three prion strains. PLoS Pathog 12:e1005551. https://doi.org/10.1371/journal.ppat.1005551
91. Arrant AE, Filiano AJ, Unger DE, Young AH, Roberson ED (2017) Restoring neuronal progranulin reverses deficits in a mouse model of frontotemporal dementia. Brain 140:1447–1465. https://doi.org/10.1093/brain/awx060
92. Arrant AE, Onyilo VC, Unger DE, Roberson ED (2018) Progranulin gene therapy improves lysosomal dysfunction and microglial pathology associated with frontotemporal dementia and neuronal ceroid lipofuscinosis. J Neurosci 38:2341–2358. https://doi.org/10.1523/JNEUROSCI.3081-17.2018
93. Beel S, Herdewyn S, Fazal R, De Decker M, Moisse M, Robberecht W, Van Den Bosch L, Van Damme P (2018) Progranulin reduces insoluble TDP-43 levels, slows down axonal degeneration and prolongs survival in mutant TDP-43 mice. Mol Neurodegener 13:55. https://doi.org/10.1186/s13024-018-0288-y

Publisher's note